NASA/CR–2010-216698

Design of Structurally Efficient Tapered Struts

Ross Messinger
The Boeing Company, Phantom Works, Huntington Beach, California

May 2010

NASA STI Program . . . in Profile

Since its founding, NASA has been dedicated to the advancement of aeronautics and space science. The NASA scientific and technical information (STI) program plays a key part in helping NASA maintain this important role.

The NASA STI program operates under the auspices of the Agency Chief Information Officer. It collects, organizes, provides for archiving, and disseminates NASA's STI. The NASA STI program provides access to the NASA Aeronautics and Space Database and its public interface, the NASA Technical Report Server, thus providing one of the largest collections of aeronautical and space science STI in the world. Results are published in both non-NASA channels and by NASA in the NASA STI Report Series, which includes the following report types:

- TECHNICAL PUBLICATION. Reports of completed research or a major significant phase of research that present the results of NASA programs and include extensive data or theoretical analysis. Includes compilations of significant scientific and technical data and information deemed to be of continuing reference value. NASA counterpart of peer-reviewed formal professional papers, but having less stringent limitations on manuscript length and extent of graphic presentations.

- TECHNICAL MEMORANDUM. Scientific and technical findings that are preliminary or of specialized interest, e.g., quick release reports, working papers, and bibliographies that contain minimal annotation. Does not contain extensive analysis.

- CONTRACTOR REPORT. Scientific and technical findings by NASA-sponsored contractors and grantees.

- CONFERENCE PUBLICATION. Collected papers from scientific and technical conferences, symposia, seminars, or other meetings sponsored or co-sponsored by NASA.

- SPECIAL PUBLICATION. Scientific, technical, or historical information from NASA programs, projects, and missions, often concerned with subjects having substantial public interest.

- TECHNICAL TRANSLATION. English-language translations of foreign scientific and technical material pertinent to NASA's mission.

Specialized services also include creating custom thesauri, building customized databases, and organizing and publishing research results.

For more information about the NASA STI program, see the following:

- Access the NASA STI program home page at *http://www.sti.nasa.gov*

- E-mail your question via the Internet to help@sti.nasa.gov

- Fax your question to the NASA STI Help Desk at 443-757-5803

- Phone the NASA STI Help Desk at 443-757-5802

- Write to:
  NASA STI Help Desk
  NASA Center for AeroSpace Information
  7115 Standard Drive
  Hanover, MD 21076-1320

NASA/CR–2010-216698

Design of Structurally Efficient Tapered Struts

Ross Messinger
The Boeing Company, Phantom Works, Huntington Beach, California

National Aeronautics and
Space Administration

Langley Research Center
Hampton, Virginia 23681-2199

Prepared for Langley Research Center
under Contract NNL04AA11B

May 2010

ACKNOWLEDGMENTS

The Boeing Company, its Phantom Works business unit, and the Phantom Works Structural Technology group acknowledge the following personnel for their valuable contribution to this task order:

Frank Biele (Boeing design)
Jeff Eichinger (Boeing materials and processes)
Dan Hansen (Boeing management oversight)
Karen Hirota (Boeing design)
Dawn Jegley (NASA technical monitor)
Mike Koharchik (Boeing analysis)
Ross Messinger (Boeing principal investigator)
Eric Olason (Park Aerospace Structures project manager)

Available from:

NASA Center for AeroSpace Information
7115 Standard Drive
Hanover, MD 21076-1320
443-757-5802

PREFACE

This report of task order NNL08AD08T of NASA contract NAS-1-NNL04AA11B, entitled Structures and Materials and Aerodynamic, Aerothermodynamic and Acoustics Technology for Aerospace Vehicles (SMAAATAV), summarizes Boeing contractor analysis efforts performed during the task order period of performance between August 7, 2008, and November 21, 2008. This report describes in detail the analytical study of two full-scale tapered composite struts and briefly describes the fabrication of two subscale demonstration struts.

ABSTRACT

This final report describes in detail the analytical study of two full-scale tapered composite struts and briefly describes the fabrication of two subscale demonstration struts. The analytical study resulted in the design of two structurally efficient carbon/epoxy struts in accordance with NASA-specified geometries and loading conditions. Detailed stress analysis was performed of the insert, end fitting, and strut body to obtain an optimized weight with positive margins. Two demonstration struts were fabricated based on a well-established design from a previous Space Shuttle strut development program.

TABLE OF CONTENTS

LIST OF FIGURES

1.0 INTRODUCTION

NASA has an enduring interest in high-performance structures for a wide variety of aerospace applications. One pervasive structural element is the structurally efficient strut, which can be used in a space frame or large assembly to support subsystems such as solar panels or propellant tanks. Composite materials are particularly suited for such struts since their unique strength and stiffness properties can be leveraged to optimize the structural efficiency of the strut. However, to fully implement this performance advantage, the composite strut should be fabricated and inspected with affordable, traceable, and repeatable processes.

The objective of this task order was to perform an analytical study of two structurally efficient, full-scale, tapered composite struts, and to fabricate a subscale strut demonstration article. As summarized below, the Boeing approach to achieve this objective was to leverage and extend recent experience on a Space Shuttle composite strut development program.

The first step of the analytical study was to identify design requirements and considerations as applicable to the analytical study, a production program, and the demonstration strut. Using these requirements and considerations, detailed design and stress analysis would determine the optimum (minimum) weight of the full-scale struts. One full-scale strut was required to carry a 44,000-pound compression load and have a 135-inch pin-to-pin length. The second strut was required to carry a compression load of 110,000 pounds and have a pin-to-pin length of 127 inches. In this report, the 44K-lb, 135-inch strut and the 110K-lb, 127-inch strut will be referred to as the 44K and 110K struts, respectively.

The approach for the subscale strut demonstration (hereinafter, demo) article was to 1) select a strut from a set of existing designs created during the Shuttle strut program, 2) fabricate at least one strut with a focus on improving laminate quality, and 3) identify process improvements. The selected strut design would be approximately half-scale, yet represent all the design features of a full-scale strut. Using the selected design, at least one demo strut would be fabricated by Park Aerospace Structures (hereinafter, Park), which participated in the Shuttle composite strut program. Based on experience from the fabrication of the demo strut(s), various process improvements would be identified and recommended for implementation during the fabrication of a future full-scale strut test article. These improvements may increase as-built composite material properties and thus further enhance strut performance.

2.0 ANALYTICAL STUDY

The analytical study consisted of the detail design and analysis of two full-scale carbon/epoxy struts in accordance with NASA-specified geometries and loading conditions.

2.1 Requirements and Considerations

The design requirements and considerations for the two struts are tabulated in Figure 2.1-1. Design requirements as specified by NASA are provided as the first four entries in the table. In addition to the geometry and load requirements, NASA required that no joints exist in the composite tube section to preclude any joint weight penalty. The remaining entries are design considerations that may have influenced the design. Parameters considered include materials, stacking sequence, thicknesses, cross-section shape, imperfections, ability to attach joints on the ends, manufacturing methods, complexity, damage tolerance, environmental degradation, and fatigue, and minimum gage. Many of these considerations were important for the Space Shuttle composite strut program (Section 3.1). Each requirement or consideration has an assumed requirement or consideration for an Altair lunar lander. Altair is an element of the NASA Exploration program to return to the Moon for extended duration missions. Each requirement or consideration is assigned a qualitative or quantitative value as appropriate for the analytical study, for a production program, and for the strut demonstration article.

An explanation of each requirement or consideration is provided in the following.

Compression load—Limit compression load for each strut was defined by NASA for the analytical study. Production struts may be designed for a wide range of loads.

Length—The pin-to-pin length of the two full-scale analytical struts was specified by NASA, and may represent the length of typical full-scale production struts in the Altair lunar lander. The demo strut was selected from the available set of Shuttle replacement strut designs. The selected strut has a length of 65.97 inches, which is about one-half length scale compared to the analytical study struts.

End fitting boundary condition—A pinned end fitting was required by NASA, which is typically implemented to ensure transmission of axial forces and to preclude transmission of bending moments.

Number of tube joints—No joints in the tube body were specified by NASA to ensure minimum weight.

Compression stability—The two struts in the analytical study were designed not to buckle under ultimate compression load.

Tension load—A tension load condition was not specified by NASA.

Reliability—Structure reliability is typically represented by a factor of safety, which is normally 1.4 for rigorously-qualified human-rated spacecraft.

Stiffness—The Altair lunar lander may have a stiffness requirement that drives the stiffness of individual structural elements. This consideration was not identified as a requirement by NASA, so the struts of the analytical study were not designed for stiffness.

Length adjustment—Production struts should be adjustable to accommodate some variation during final assembly. The Shuttle replacement struts were adjustable with a threaded post and lock nuts. A more weight-efficient and reliable approach is to machine the end fitting to the precise length or shape during final assembly.

Strut Design Requirements and Considerations		Design implementation		
Requirement/ Consideration	**System-level (Altair) requirement**	**Analytical Study**	**Production**	**Demo strut**
Compression load (requirement)	Various	A: 44,000 lb (limit) B: 110,000 lb (limit)	AR	16,464 lb (ultimate)
Length (requirement)	Various	A: 135 inches B: 127 inches (from center of ball end fittings)	AR	65.97-inch pin-to-pin max. length (60.88-inch tube length)
End fitting boundary condition (requirement)	Accommodate various attachment requirements	A: pinned on both ends B: pinned on both ends	AR	NI
Number of tube joints (requirement)	Minimize weight	0	0	0
Compression stability	No buckling at ultimate compression load	No buckling at ultimate compression load	No buckling at ultimate compression load	NI
Tension load	Various	NI	AR	18,325 lb (ultimate)
Reliability	Ultimate factor of safety	1.4	1.4 (1.2 proof FS)	1.4
Stiffness	System-level stiffness or modal frequency: Component modal frequency	NI (strength-driven design and material)	AR	NI (IM7/8552 laminate modulus of 16.2 msi)
Length adjustment	Final assembly dimensional tolerances	Machine end fitting on final assy	Final machine end fitting or node feature	NI (no adjustment for screw-on end fittings)
Dimensional accuracy	Final assembly dimensional tolerances	Integrated insert and end fitting, see length adjustment	Integrated insert and end fitting, see length adjustment	NI (screw-on end fittings not dimensionally accurate)
Straightness	Minimize end-to-end bowing	NI (assume no bowing)	AR (assume max allowable bowing)	NI
Tube internal pressure	Accommodate 14.7psig max. during launch	NI (relieving)	AR	NI
Operating temperature	Acceptable properties at min/max temperatures during (Altair) mission	NI (assume ambient temp.only)	AR (dependent on system design and material)	NI (IM7/8552 temperature limit (-250F to +250 F)
Operating temperature change	Minimize thermal displacement	NI (strut tube IM7/8552 material has low CTE)	AR	NI (strut tube IM7/8552 material has low CTE)
Fatigue	Accommodate (Altair) mission thermo-mechanical cycles	NI (assume not a design driver)	AR	NI
Low-(high) energy impact/damage tolerance	Maximize residual strength after nondetectable impact damage	Interspersed 90 degree plies (90/0(4)/90/0(4)/90)	AR (Ply layup that balances mechanical properties and DT)	Interspersed 90 degree plies (90/0(4)/90/0(4)/90)
Non-destructive inspectability	Accommodate damage/flaw detection	NI	Thermography and C-scan (with standards)	Thermography and C-scan (no standards)
Ground operations damage detection	Minimize nondetectable technician-induced impact damage during ground ops	NI	Fiberglass cover ply, acoustic emission sensor, etc.	NI
Laminate quality	Maximize laminate properties with minimum material property knockdowns	Pristine (no knockdowns)	multiple debulks, autoclave cure	Multiple autoclave debulks maximized laminate quality
Dissimilar material compatibility	No degradation at component interfaces	Compatible Ti insert and Gr/Ep tube	Compatible Ti insert and Gr/Ep tube	Compatible Ti insert and Gr/Ep tube
Material environmental effects and compatibility (durability)	Minimize degradation due to radiation, outgassing, etc.	NI	AR (coatings, etc)	NI
Subsystem integration	Ability to attach wiring, secondary structure, instrumentation, insulation, etc. to strut tube	NI	AR	NI
Insert attachment to composite tube	High reliability, and high failure and degradation tolerance	Sinusoidal insert per PAS patent (no adhesive bondline failure modes)	Sinusoidal insert per PAS patent	Sinusoidal insert per PAS patent
Number of struts attached to single node	11 max.	Tapered strut tube ends, with end fitting to attach 11 struts (max) to one node	AR	Tapered strut tube ends
End fitting type	Accommodate variety of end fittings with	NI	AR (machine ball, clevis, etc from blank)	screw-on ball and clevis
Process repeatability	Minimize material property knockdowns due to process variability	No material property knockdowns	Automated tow placement	PAS manual process
Process traceability	Maximize part reliability and performance	NI	Complete use of documentation and specifications	Limited use of documentation and specifications
Tube cross section	Maximize structural efficiency while considering subsystem attachment	Circular	AR (circular, square, open section, etc)	Circular
Diameter	Avoid interference with adjacent subsystems and structures	Optimize for min. mass A: 6.0-inch ID B: 6.5-inch ID	AR	2.233-inch ID
Minimum gage	Tube wall thickness required for adequate damage tolerance	NI	AR	NI ((90/0(4)/90/0(4)/90) layup above min gage)

Figure 2.1-1. Design Requirements and Considerations

Straightness—Excessive bowing will significantly reduce compression strength and stiffness. The Space Shuttle replacement struts had a bowing requirement of less than 0.030-inch plus 0.001 inch for each additional inch above 30 inches.

Tube internal pressure—The strut tubes will experience an internal positive pressure during launch into low-Earth orbit. This load was ignored for the analytical study struts.

Operating temperature—The struts may experience a wide range of temperatures, depending on the degree of thermal protection and location of the struts in the Altair lander or other spacecraft. Without further definition, the analytical study assumed an ambient temperature.

Operating temperature change—A change in temperature will induce thermal displacements and stresses that can affect overall stiffness, strength, and dimensional accuracy. Temperatures changes will depend on the degree of thermal protection and location of the struts in the Altair lander or other spacecraft.

Fatigue—The Altair lander may experience a series of thermal-mechanical load cycles, while in low-Earth orbit, during transfer to lunar orbit, and on the lunar surface. These load cycles were not defined at this time, so were not considered in the analytical study.

Low-(high) energy impact/damage tolerance—The primary source of damage is expected to occur during final assembly and ground operations. The strut body laminate should be designed to tolerate such low-energy ground impacts. Any low- or high-energy impact damage during flight operations is unlikely given the expected environmental protection and surrounding subsystems and in the Altair lander.

Nondestructive inspectability—After cure, the struts need to be inspectable to ensure laminate quality.

Ground operations damage detection—Impact damage should be detectable either during the impact event or during subsequent inspection. For example, the Space Shuttle replacement strut program investigated the use of a single fiberglass composite cover ply that readily and visually delaminated from the carbon/epoxy strut body when subjected to local impact.

Laminate quality—The strut body should have a minimum of wrinkles, voids, and porosity to maximize mechanical properties and minimize associate analytical knockdown factors..

Process repeatability—The production fabrication process should be highly repeatable to minimize statistical knockdowns from material properties. The analytical study assumed no knockdown from such variability, other than that inherent in the A-basis allowable values.

Dimensional accuracy—The Altair lander may require well-controlled dimensional tolerances to accurately support numerous subsystems. The production strut design incorporates a spherical node that is integrated with patented Park end fitting. The spherical node is tightly integrated with the node.

Dissimilar material compatibility—Direct contact between carbon-based composites and metals such as aluminum should be avoided to preclude galvanic corrosion. The demo struts used compatible titanium end fittings.

Material environmental effects and compatibility (durability)—The demo strut tube IM7/8552 material will be exposed to deep space vacuum and radiation during an Altair mission for period of about two weeks.

Subsystem integration—Ability to attach wiring, secondary structure, instrumentation, and insulation can affect the strut design. Since there is no current definition of this integration, the analytical struts did not consider these attachments:

Insert attachment to composite tube—Typical end fittings in a composite strut are metallic. The Park end fitting features a unique corrugated surface to create a mechanical lock between the end fitting and composite overwrap.

Number of struts attached to single node—As many as 11 struts may be attached to a single node. The tapered ends of the analytical and demo strut designs allows close nesting of struts.

End fitting type—The Altair lunar lander may have various structural requirements that will are satisfied with ball, clevis, or other end fittings.

Process repeatability—Manual fabrication processes are inherently more variable than automated processes. Higher resulting material properties knockdowns lower strut performance.

Process traceability—Documentation of materials and process ensures quality and repeatability. Altair will likely require the most rigorous traceability of the production struts.

Tube cross section—While the analytical and demo struts used a circular cross section, other sections may be more suitable for specific purposes in the Altair lander.

Diameter—The compression stability of the strut is largely determined by the body diameter, but may be constrained by adjacent subsystems in the Altair/spacecraft assembly.

Minimum gage—Lightly-loaded struts may only need a few laminate plies, which will be constrained by damage tolerance or producibility.

2.2 Design

Based on the applicable requirements and considerations in Section 2.1, detailed design of the 44K and 110K struts was performed to document the results of the detailed analysis in Section 2.3.

2.2.1 44K Strut

The 44K strut assembly consists of a composite body and two end fittings (Figure 2.2.1-1). The composite body is a single-piece laminate with tapered ends that capture the two end fittings. The length between the centers of the two ball end fittings is 135.0 inches. The cylindrical portion of the body has an inner diameter of 6.00 inches.

The material specification and ply layup of the 44K strut are detailed in Figure 2.2.1-2. The carbon/epoxy materials are IM7/8552-1 prepreg tow and IM7/8552-2 prepreg tape, which are used for the circumferential (90-deg) and axial (0-deg) plies, respectively. The tube layup is $(90,0_4,90,0_3,90,0_4,90)$ for a total of 15 plies. The ply layup in the end fitting region consists of the tube plies and additional hoop (90-deg) plies that secure the tube plies to the end fitting.

The end fitting of the 44K strut is made of 6Al-4V titanium alloy and consists of an integral insert and ball (Figure 2.2.1-3). The insert design, patented by Park (6,379,763), has three corrugations which create a high-performance and high-reliability mechanical lock between the composite and insert. The spherical ball portion of the end fitting is installed into a node to provide a pinned (zero moment) end condition. The ball is shown in an outlined block, indicating that the ball is final machined from a blank after the end fitting is cured with the composite body.

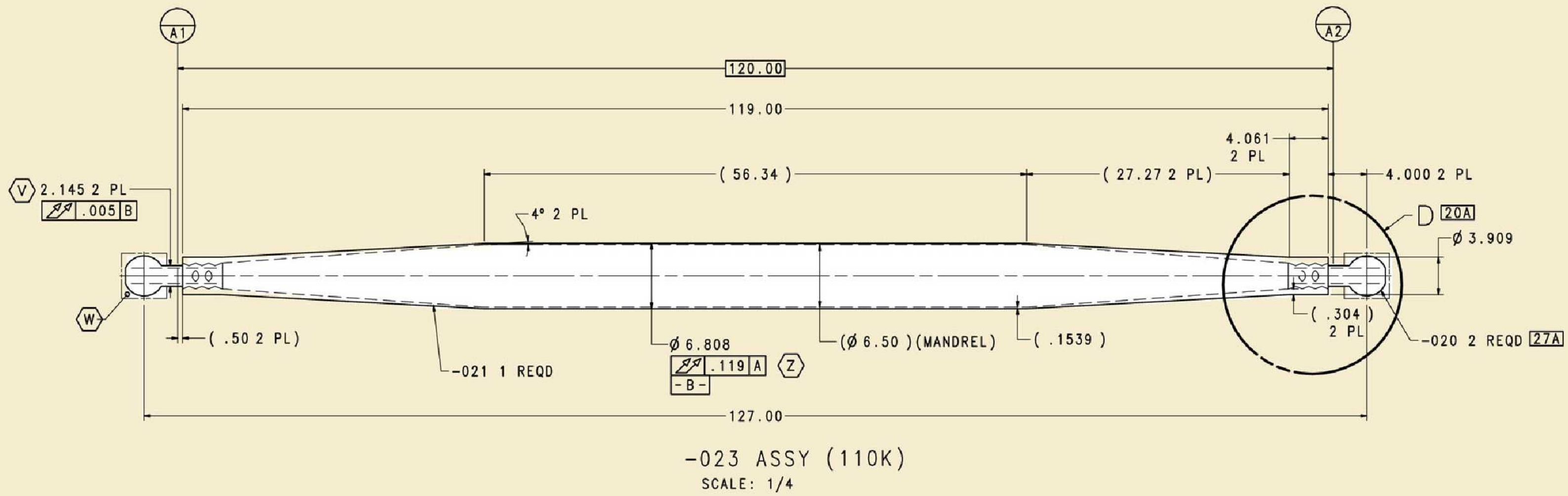

Figure 2.2.1-1. 44K Strut Assembly Design

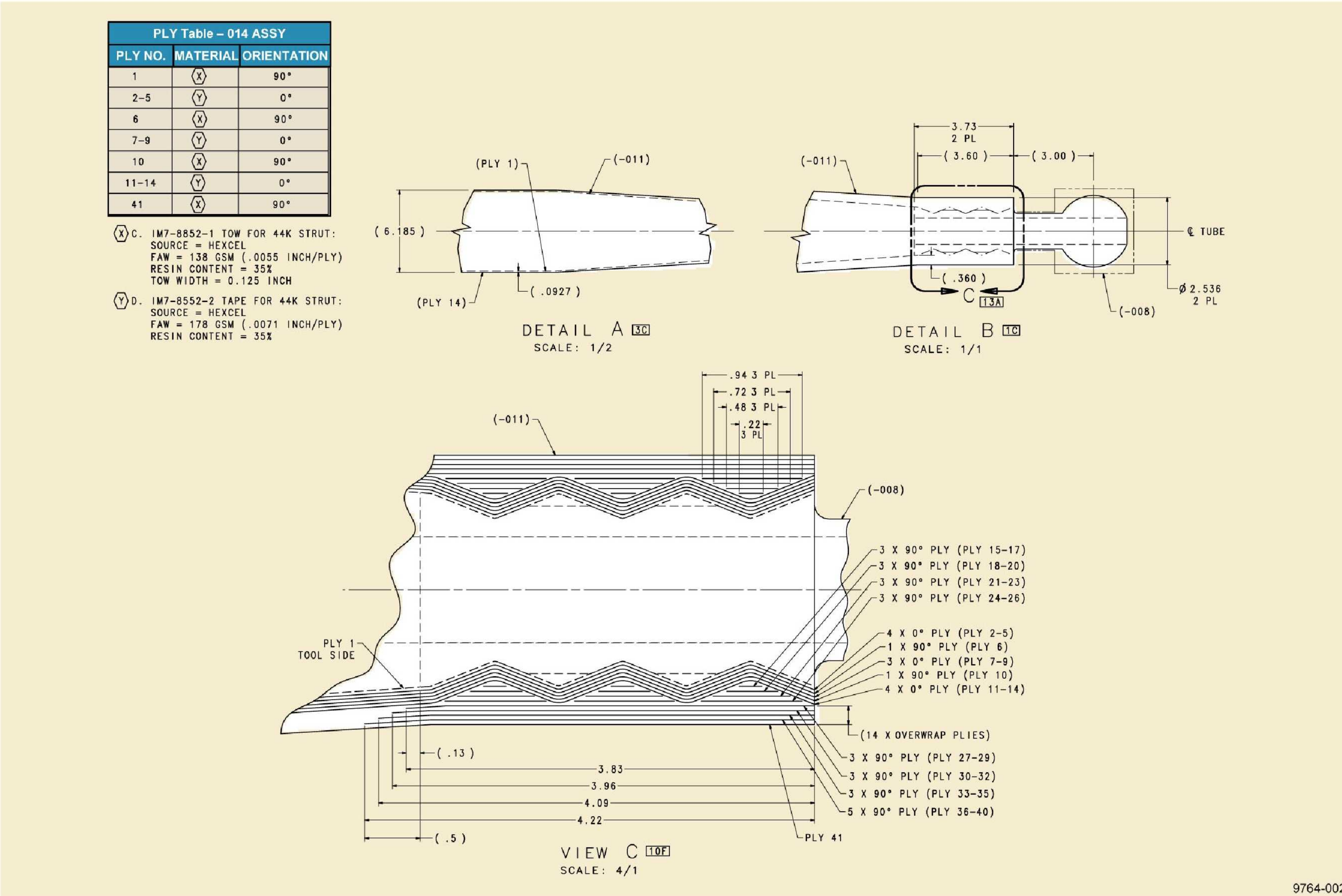

PLY Table – 014 ASSY		
PLY NO.	MATERIAL	ORIENTATION
1	X	90°
2-5	Y	0°
6	X	90°
7-9	Y	0°
10	X	90°
11-14	Y	0°
41	X	90°

Figure 2.2.1-2. 44K Strut Ply Layup

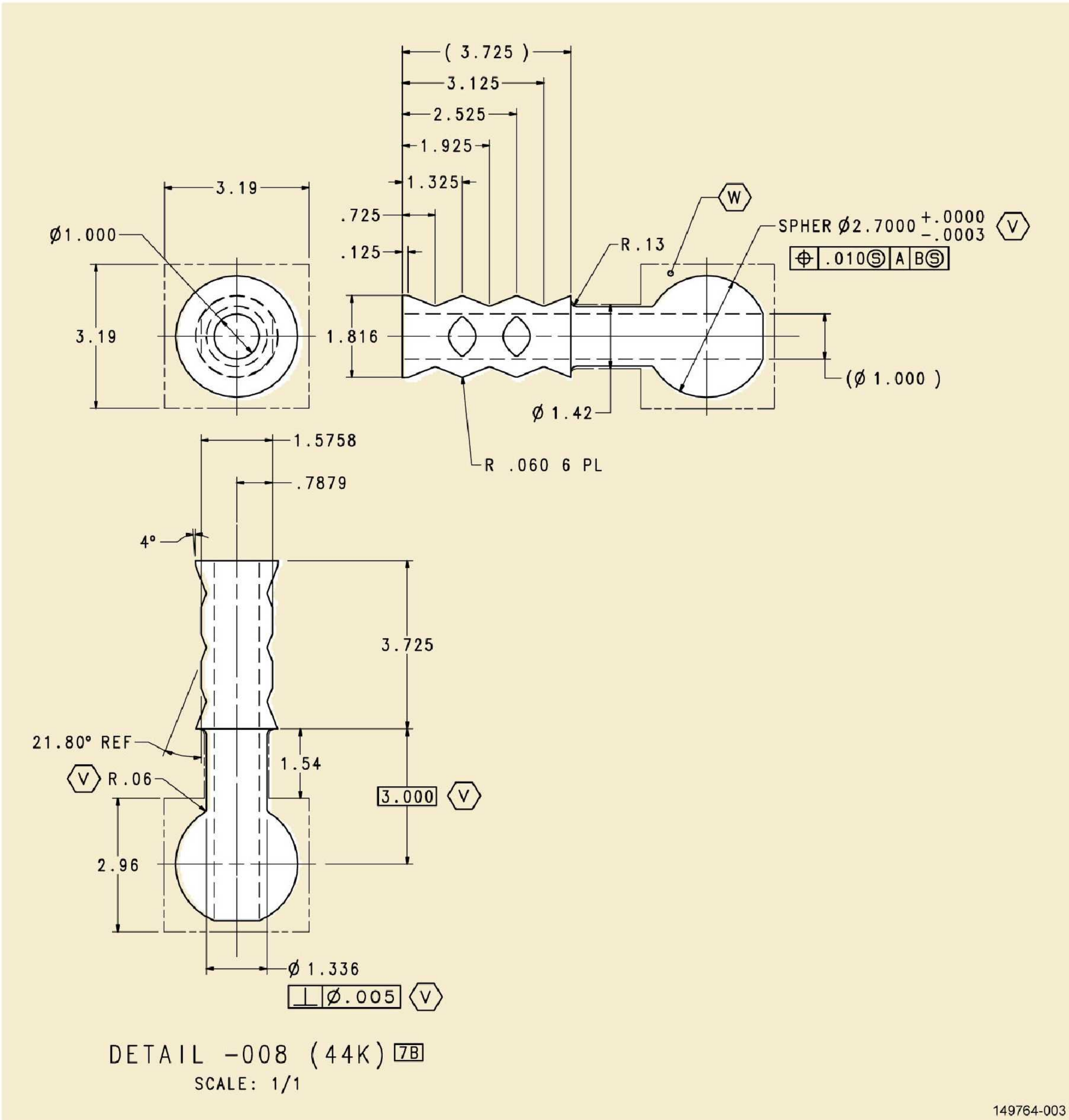

Figure 2.2.1-3. 44K Strut End Fitting Detail Design

2.2.2 110K Strut

The 110K strut assembly consists of a composite body and two end fittings (Figure 2.2.2-1). The composite body is a single-piece laminate with tapered ends that capture the two end fittings. The length between the centers of the two ball end fittings is 127.0 inches. The cylindrical portion of the body has an inner diameter of 6.50 inches.

The material specification and ply layup of the 110K strut are detailed in Figure 2.2.2-2. The carbon/epoxy materials are IM7/8552-1 prepreg tow and IM7/8552-2 prepreg tape, which are used for the circumferential (90-deg) and axial (0-deg) plies, respectively. The tube layup is $(90,0_3,90,0_3,90,0_4,90,0_4,90,0_3,90,0_3,90)$ for a total of 27 plies. The ply layup in the end fitting region consists of the tube plies and additional hoop (90-deg) plies that secure the tube plies to the end fitting.

The end fitting of the 110K strut is made of 6Al-4V titanium alloy and consists of an integral insert and ball (Figure 2.2.2-3). The insert design, patented by Park (6,379,763), has three corrugations, which create a high-performance and high-reliability mechanical lock between the composite and insert. The spherical ball portion of the end fitting is installed into a node to provide a pinned (zero moment) end condition. The ball is shown in an outlined block, indicating that the ball is final machined from a blank after the end fitting is cured with the composite body.

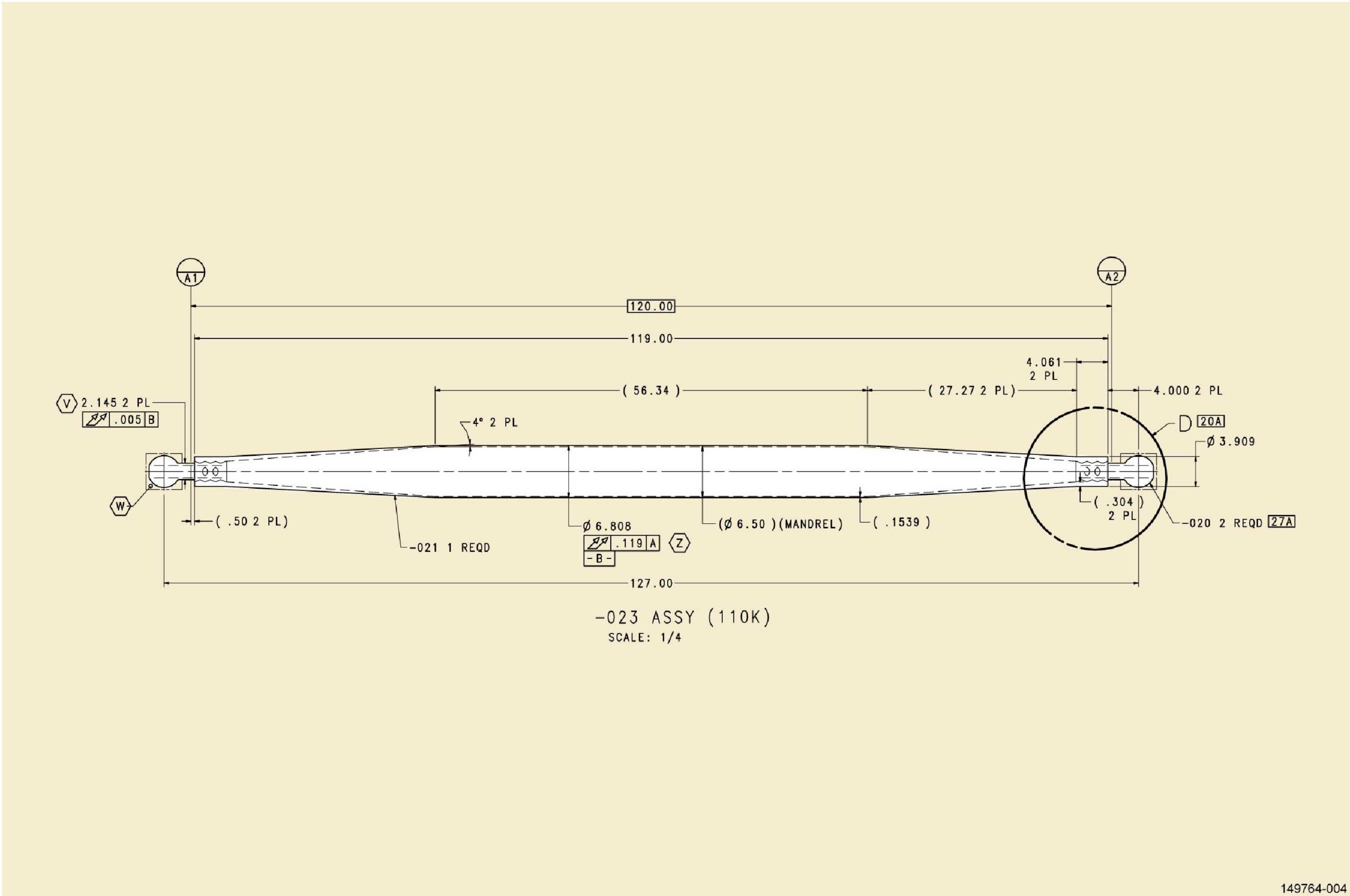

Figure 2.2.2-1. 110K Strut Assembly Design

PLY Table – 023 ASSY		
PLY NO.	MATERIAL	ORIENTATION
1	X	90°
2-4	Y	0°
5	X	90°
6-9	Y	0°
10	X	90°
11-14	Y	0°
15	X	90°
16-19	Y	0°
20	X	90°
21-23	Y	0°
80	X	90°

X F. IM7-8852-1 TOW FOR 110K STRUT:
SOURCE = HEXCEL
FAW = 138 GSM (.0055 INCH/PLY)
RESIN CONTENT = 35%
TOW WIDTH = 0.125 INCH

Y G. IM7-8552-2 TAPE FOR 110K STRUT:
SOURCE = HEXCEL
FAW = 178 GSM (.0071 INCH/PLY)
RESIN CONTENT = 35%

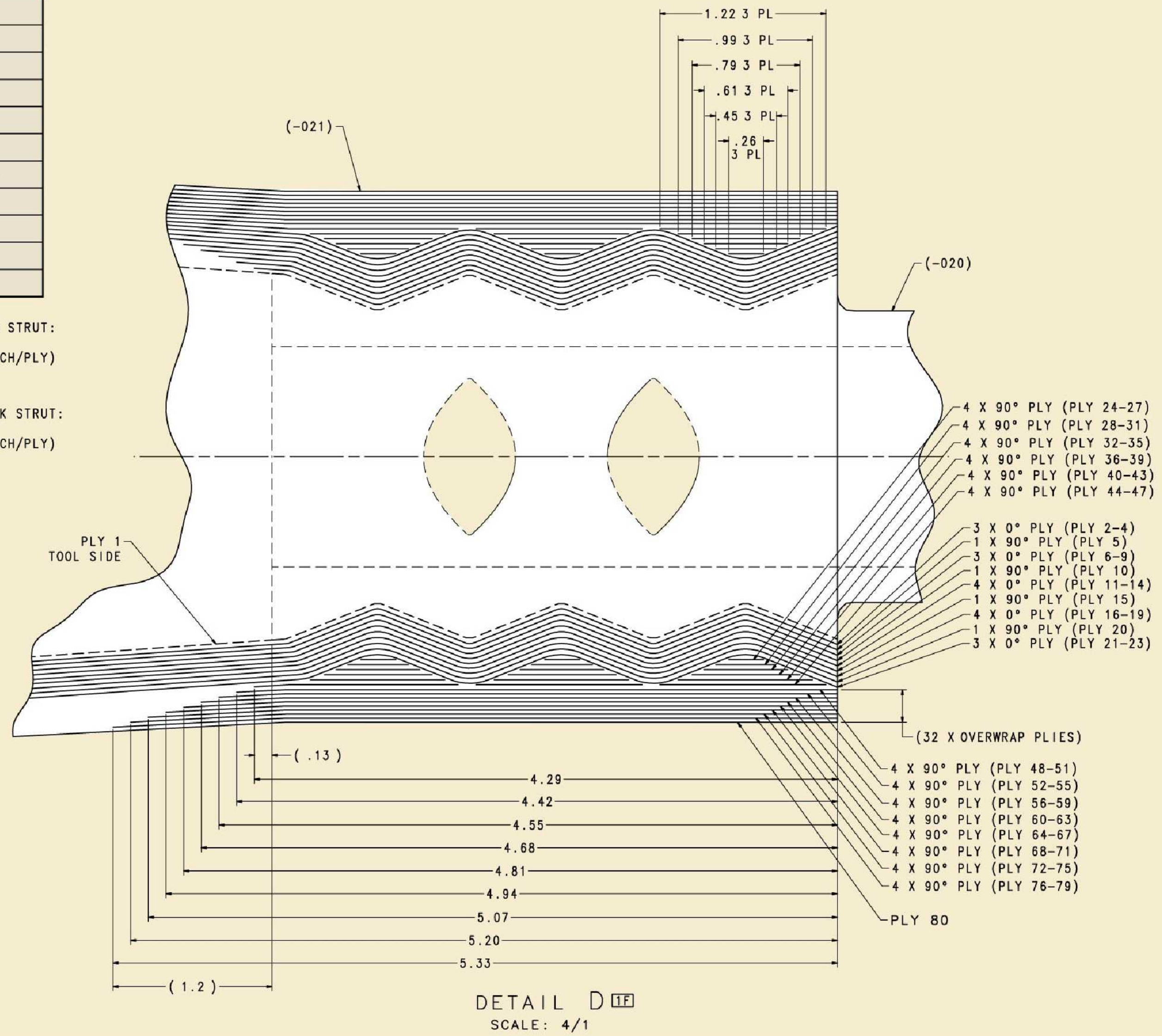

Figure 2.2.2-2. 110K Strut Ply Layup

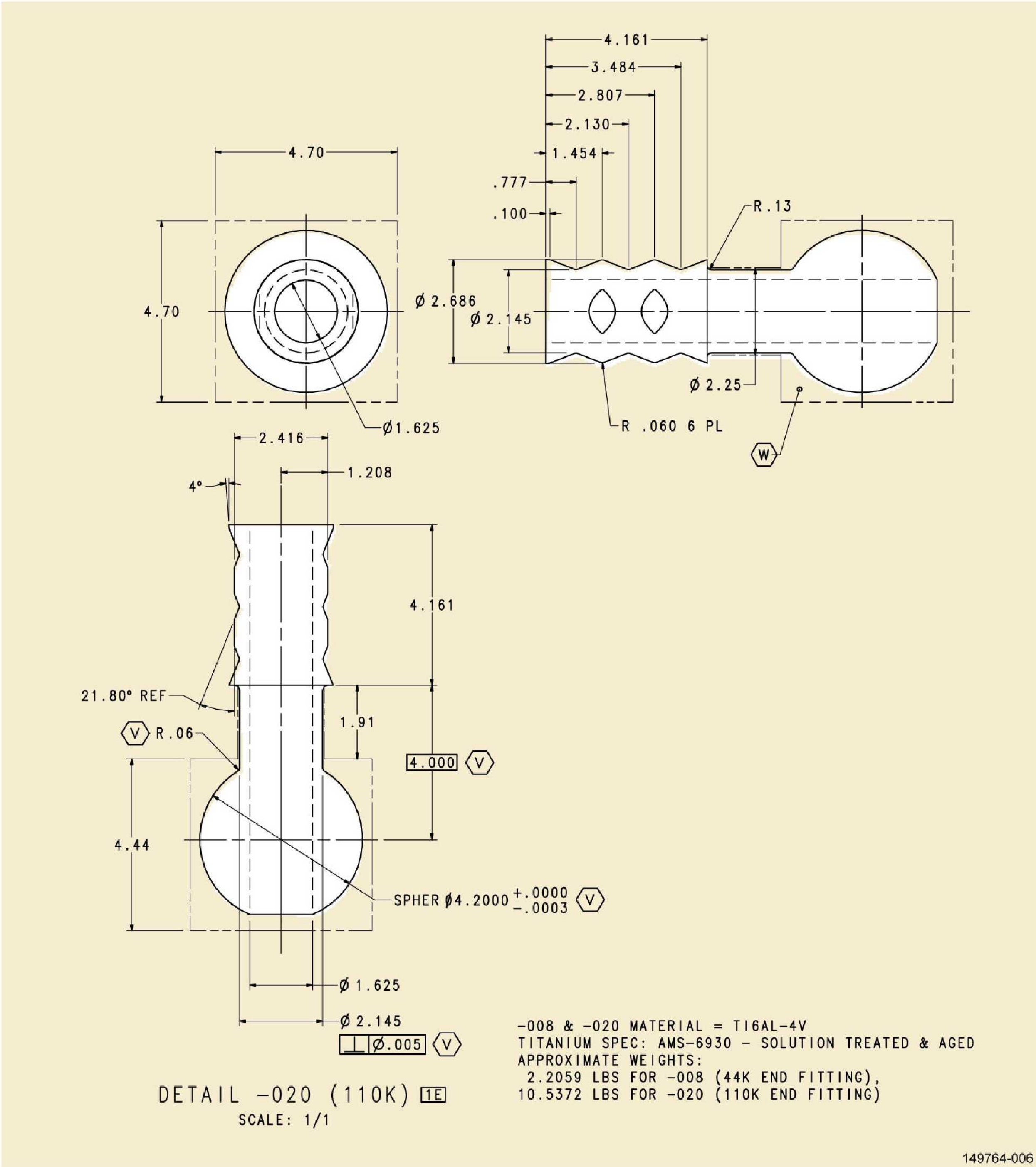

Figure 2.2.2-3. 110K Strut End Fitting Detailed Design

2.2.3 Node Attachment

The ball end fitting described in Sections 2.2.1 and 2.2.2 is but one of a wide variety of end fittings that can be incorporated into the strut assembly. The ball end fitting would be installed into a spherical recess in the receiving node. Other examples of node attachment options include a post, receiving ball, single clevis, double clevis, and receiving cruciform (Figure 2.2.3-1). The figure also illustrates how these end fittings can be combined to create complex assemblies. Furthermore, each end of the strut can have a unique end fitting. To illustrate this feature, the demo strut may include the ball end fitting described in Sections 2.2.1 and 2.2.2 on one end, and/or the clevis end fitting on the other (Section 3.0).

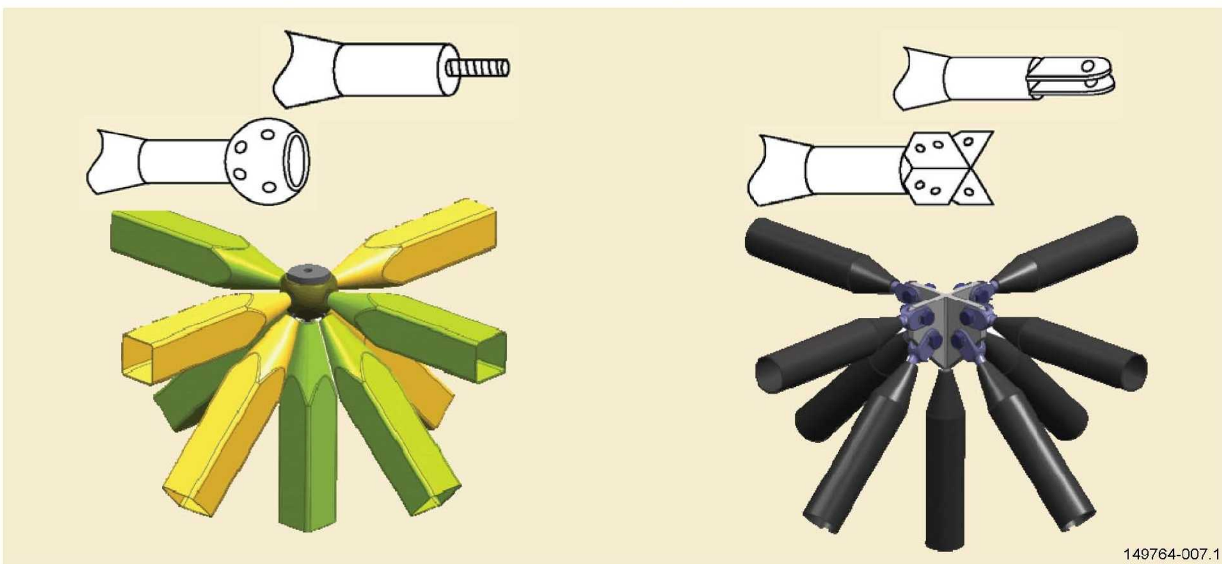

Figure 2.2.3-1. Node Attachment Concepts

2.3 Analysis

Detailed stress analysis of the 44K and 110K struts was performed to obtain optimized (minimum) weights. The sizing satisfies the requirements and considerations applicable to the analytical study as described in Section 2.1. The analysis began with the optimization (minimum-weight) of the strut tube diameter. Given the optimum diameter, detailed stress analysis was performed to confirm buckling strength and other positive margins. The optimized weight of the two struts is summarized in Figure 2.3-1. The following analysis shows that both struts have positive margins of safety and satisfy other important parameters (Figure 2.3-2).

	Weight (lb)	
	44K Strut	110K Strut
Body	13.31	23.28
Insert	1.20	3.56
Ball	1.50	5.40
Total	16.01	32.24

Figure 2.3-1. 44K and 110K Strut Weight Summary

	MS/Value	
	44K Strut	110K Strut
End fitting bearing	5.58	5.14
End fitting hoop stress	0.52	0.33
Insert tension stress	0.30	0.30
Insert hoop stress	0.52	0.33
Insert joint shear stress (<5000 psi)	3856 psi	4997 psi
Strut buckling, Pult > Pcr (lb)	64,451> 61,600	160,623 > 154,000
First natural frequency, f1 (Hz)	63	79
Compression	3.63	2.31
Crippling/Local Instability	0.26	0.11

Figure 2.3-2. Summary of Margins of Safety and Critical Parameters

2.3.1 Strut Diameter Optimization

2.3.1.1 44K Strut

The 44K strut diameter optimization was performed by Park using an established Excel-based analysis method. The diameter of the constant-section of the strut body and the number of tube plies were varied to achieve the required compression strength (Figure 2.3.1.1-1). Based on those results, the minimum weight is shown in Figure 2.3.1.1-2 when the tube inner diameter is 6.0 inches and the number of plies is 10.

ID (in)	No. of 0-deg Plies	OD (in)	Failure Mode	Weight (lb)
4.0	27	4.47	Buckling	24.41
4.5	20	4.85	Buckling	20.32
5.0	15	5.27	Buckling	17.37
5.5	12	5.72	Buckling	15.39
6.0	10	6.19	Crippling	14.61
6.5	10	6.69	Crippling	15.66
7.0	9	7.17	Crippling	15.56
7.5	9	7.67	Crippling	16.53
8.0	9	8.17	Crippling	17.51
8.5	9	8.67	Crippling	18.48
9.0	9	9.17	Crippling	19.45
9.5	9	9.67	Crippling	20.42
10.0	9	10.17	Crippling	21.40

Figure 2.3.1.1-1. 44K Strut Optimization Results

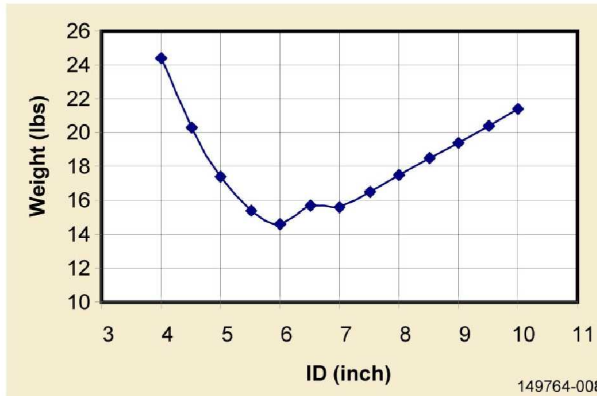

Figure 2.3.1.1-2. 44K Strut Weight as a Function of Diameter

2.3.1.2 110K Strut

The 110K strut diameter optimization was performed using an established Excel-based analysis method at Park. The diameter of the constant-section of the strut body and the number of tube plies were varied to achieve the required compression strength (Figure 2.3.1.2-1). Based on those results, the minimum weight is shown in Figure 2.3.1.2-2 when the tube inner diameter is 6.5 inches and the number of plies is 17.

ID (in)	No. of 0-deg Plies	OD (in)	Failure Mode	Weight (lb)
4.0	52	4.89	Buckling	47.30
4.5	40	5.19	Buckling	40.67
5.0	31	5.54	Buckling	35.44
5.5	24	5.92	Buckling	30.64
6.0	19	6.34	Buckling	27.33
6.5	17	6.80	Crippling	26.27
7.0	17	7.30	Crippling	27.83
7.5	17	7.80	Crippling	28.39
8.0	16	8.28	Crippling	29.70
8.5	16	8.78	Crippling	31.18
9.0	16	9.28	Crippling	32.67
9.5	15	9.77	Crippling	32.69
10.0	15	10.27	Crippling	34.09
10.5	15	10.77	Crippling	35.50
11.0	15	11.27	Crippling	36.91
11.5	14	11.75	Crippling	36.56
12.0	14	12.25	Crippling	37.89

Figure 2.3.1.2-1. 110K Strut Optimization Results

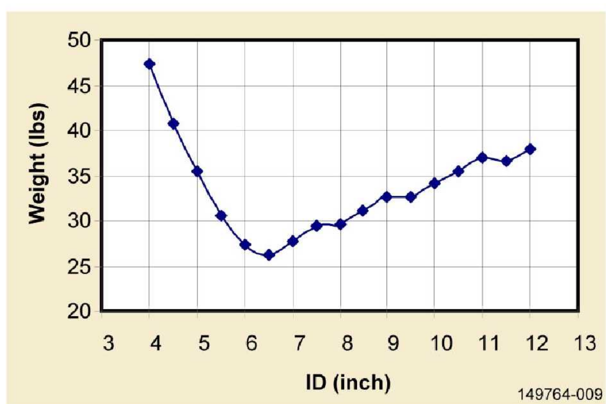

Figure 2.3.1.2-2. 110K Strut Weight as a Function of Diameter

2.3.2 End Fitting Analysis

The end fitting (Figure 2.3.2-1) is a titanium part consisting of a shaft with a ball end. An axial hole through the center is used during fabrication for access to and removal of the drill rod and plaster mandrel.

Material Properties

6Al – 4V annealed titanium

E = 16,000,000 psi

F_{TU} = 130,000 psi

F_{CY} = 126,000 psi

F_{brU} = 191,000 psi

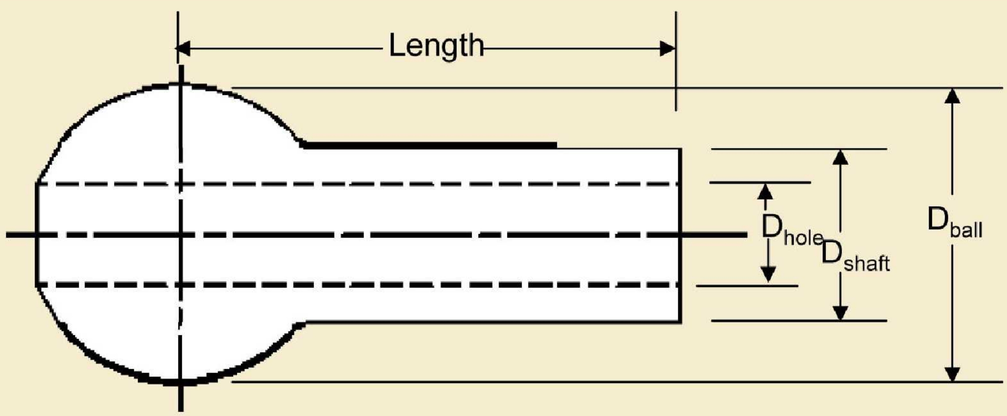

End Fitting Dimensions

	44k	110k
D_{ball} [in]	2.7	4.2
D_{shaft} [in]	1.336	2.145
D_{hole} [in]	1.0	1.625
Length [in]	3.0	4.0

149764-010

Figure 2.3.2-1. End fitting dimensions

Compression

Compression loads are transmitted to the end of the ball through surface bearing, and distributed over the effective surface area.

$$\theta_{min} = \sin^{-1}\left(\frac{D_{hole}}{D_{ball}}\right)$$

$$\theta_{max} = 45°$$
$$\theta_{ave} = (\theta_{max} + \theta_{max}) / 2$$

	44k	110k
θ_{min}	21.74°	22.76°
θ_{max}	45°	45°
θ_{ave}	33.37°	33.88°

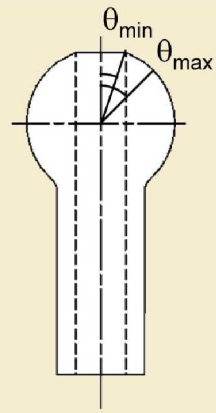

149764-011

Buckling

Buckling of the end fitting depends on the stiffness of the rest of the strut and therefore cannot be performed independently of the strut. The end fitting is included in the overall strut buckling analysis.

Surface Bearing

Compression loads are distributed over the effective surface contact area at the end of the ball. The surface area of a spherical cap of radius r and height h is given by

$$A = 2\pi rh$$

In the case of the ball end, this will be the area of the cap above θ_{max} minus the area above θ_{min}

$$A = 2\,\pi\,(D_{ball}/2)\,[(D_{ball}/2)\,(1 - \cos\theta_{max})] - 2\,\pi\,(D_{ball}/2)\,[(D_{ball}/2)\,(1 - \cos\theta_{min})]$$

	44k	110k
A	2.54 in²	5.96 in²

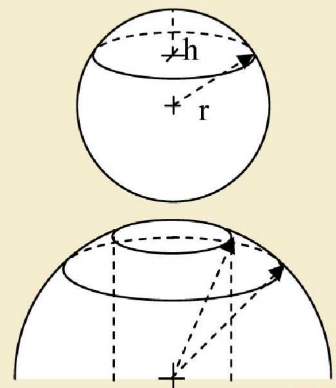

149764-012

Assuming a frictionless interface, the bearing forces act normal to the surface of the ball

$$RbULT = 1.4P_{app} / \cos \theta_{ave}$$

	44k	110k
R_{bULT}	73,760 lbs	185,498 lbs

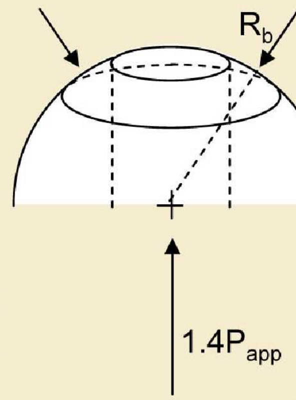

149764-013

The bearing stress is then

$\sigma_{brU} = R_{bULT} / A$

For the 44k strut,

$\sigma_{brU} = 73{,}760 / 2.54 = 29{,}040$ psi

MS = 191,000 / 29,040 – 1 = 5.58

For the 110k strut,

$\sigma_{brU} = 185{,}498 / 5.96 = 31{,}124$ psi

MS = 191,000 / 31,124 – 1 = 5.14

Hoop Stress

The radial component of the contact force will result in a hoop stress in the end of the ball. The minimum radius of the annular section is the radius of the hole.

The maximum radius is given by

$r_{max} = (D_{ball}/2) \sin \theta_{max}$

and the average radius is the radius at the centroid of the (approximate) triangle

$r_{ave} = r_{min} + (r_{max} - r_{min}) / 3$

the running force is then the radial force divided by the average circumference

$R_h = R_{bULT} \sin \theta_{ave} / 2\pi r_{ave}$

	44k	110k
r_{min}	0.5 in	0.8125 in
r_{max}	0.9546 in	1.4849 in
r_{ave}	0.6515 in	1.0366 in
R_h	9910 lb/in	15876 lb/in

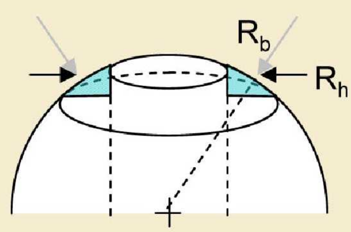

149764-014

The cross-sectional area of the ring is determined from the areas of the various segments

$$A_1 = \tfrac{1}{2}\,(D_{ball}/2)^2 * [2\theta_{max} - \sin(2\theta_{max})]$$
$$A_2 = \tfrac{1}{2}\,(D_{ball}/2)^2 * [2\theta_{min} - \sin(2\theta_{min})]$$
$$A_3 = D_{hole}\,[(D_{ball}/2)\cos\theta_{min} - (D_{ball}/2)\cos\theta_{max}]$$
$$A_4 = (A_1 - A_2 - A_3)/2$$

	44k	110k
A_1	0.5201 in^2	1.2586 in^2
A_2	0.0645 in^2	0.1786 in^2
A_3	0.2994 in^2	0.7337 in^2
A_4	0.0781 in^2	0.1731 in^2

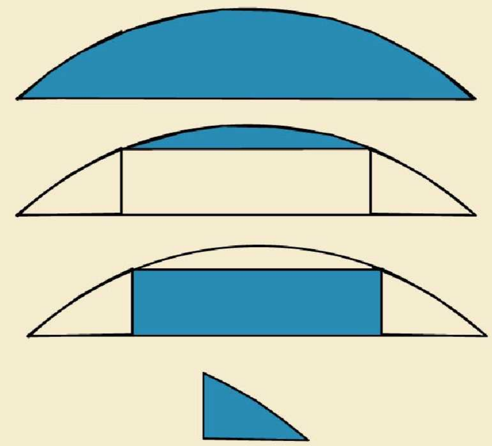

149764-015

The hoop stress is then given by

$\sigma_{hoop} = R_b\, r_{ave} / A_4$

For the 44k strut,

$\sigma_{hoop} = 9910 * 0.6515 / 0.0781 = 82{,}641$ psi

MS = 126,000 / 82,641 – 1 = 0.52

For the 110k strut,

$\sigma_{hoop} = 15{,}876 * 1.0366 / 0.1731 = 95{,}060$ psi

MS = 126,000 / 95,060 – 1 = 0.33

2.3.3 Insert Analysis

The strut insert is a titanium part with a basically cylindrical shape (Figure 2.3.3-1). The outer surface consists of a series of peaks and valleys. The strut body laminate is mechanically locked into these features by the overwrap plies, eliminating the need for adhesives or fasteners to transmit the load from the metal end fitting to the composite strut body. The hole through the center is used during fabrication for access to and removal of the drill rod and plaster mandrel.

Material Properties

6Al – 4V annealed titanium

FTU = 130 ksi

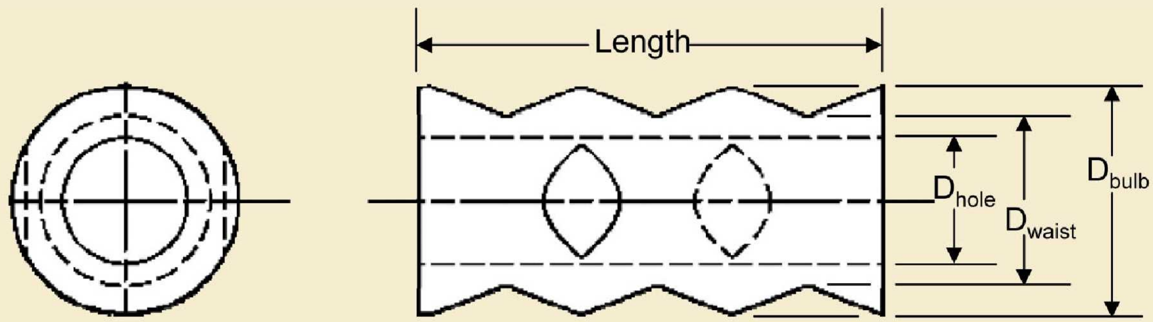

Dimensions

	44k	110k
D_{waist} [in]	1.336	2.145
D_{bulb} [in]	1.772	2.686
D_{hole} [in]	1.000	1.625
Length [in]	3.272	4.061

149764-016

Figure 2.3.3-1. Insert dimensions

Assuming the insert reacts the entire tension load (neglecting any load transmitted to the composite by adhesion or friction), stress at the waist is given by

$$\sigma = P/A = \frac{P}{\frac{\pi}{4}\left(D_{waist}^2 - D_{hole}^2\right)}$$

For the 44k strut,

$$\sigma = \frac{1.4 * 44{,}000}{\frac{\pi}{4}\left(1.336^2 - 1.000^2\right)} = 99{,}926 \text{ psi}$$

MS = 130,000 / 99,926 – 1 = 0.30

For the 110k strut,

$$\sigma = \frac{1.4 * 110{,}000}{\frac{\pi}{4}\left(2.145^2 - 1.625^2\right)} = 100{,}020 \text{ psi}$$

MS = 130,000 / 100,020 – 1 = 0.30

In addition to the tensile stress calculation, a "joint shear" calculation is performed by the vendor, with a maximum equivalent shear stress design limit of 5,000 psi.

The shear area is determined at the average diameter of the insert:

$A = \pi\, D_{ave}\, L = \pi\, [(D_{waist} + D_{bulb})/2]\, L$

For the 44k strut,

$A = \pi\, [(1.336 + 1.772)/2]\, (3.272) = 15.974\ in^2$

$\tau = P/A = 1.4 * 44{,}000 / 15.974 = 3856$ psi

For the 110k strut,

$A = \pi\ [(2.145 + 2.686)/2]\ (4.061) = 30.817\ in^2$

$\tau = P/A = 1.4 * 110{,}000 / 30.817 = 4997$ psi

In both cases, the equivalent shear stress is below the design limit of 5000 psi. A margin of Safety is not calculated since this is a design limit and not a true material allowable.

2.3.4 Buckling Analysis

A Newmark buckling analysis method was used to account for the variable cross-section of the strut. This iterative approach begins with an assumed buckling mode shape; each successive iteration generates a mode shape and corresponding buckling load. The iteration has converged when the difference in successive buckling load predictions is within the desired accuracy.

The strut is divided axially into elements and nodes, such that a node lies at each critical change in geometry (such as the transition between the end fitting and the composite strut body). Smooth transitions, such as those between tapered composite sections and straight composite sections, do not require a node to be located at the transition.

Material Properties (A-basis)

IM7-8552 Gr/E

$F_{CU}^{L} = 191.0$ ksi

$E_{longitudinal} = 21{,}000{,}000$ psi

$E_{transverse} = 1{,}100{,}000$ psi

$\rho = 0.0555\ lb/in^3$

2.3.4.1 44K Strut

The 44K strut is divided into 90 axial segments, located in the end fitting, insert, taper, and straight sections of the strut. Given the strut length of 135 inches, this corresponds to a segment length of 1.5 inches. Along with dividing evenly into the overall strut length, this segment length also divides evenly into the 3 inch length of the end fitting, conveniently placing a node at the transition between the end fitting and strut body.

End Fitting Segments

The titanium end fitting portion is analyzed as a straight cylindrical shaft – the added material at the ball is neglected. This assumption is only slightly conservative, since the properties near the end have little effect on the buckling capability.

$E = 160{,}000{,}000$ psi

$I = \pi/4\ (r_o^4 - r_i^4) = \pi/4\ ((D_{shaft}/2)^4 - (D_{hole}/2)^4)$

$I = \pi/4\ [(1.336 / 2)^4 - (1.0 / 2)^4] = 0.1073\ in^4$

$EI = 1{,}716{,}766\ lb\text{-}in^2$

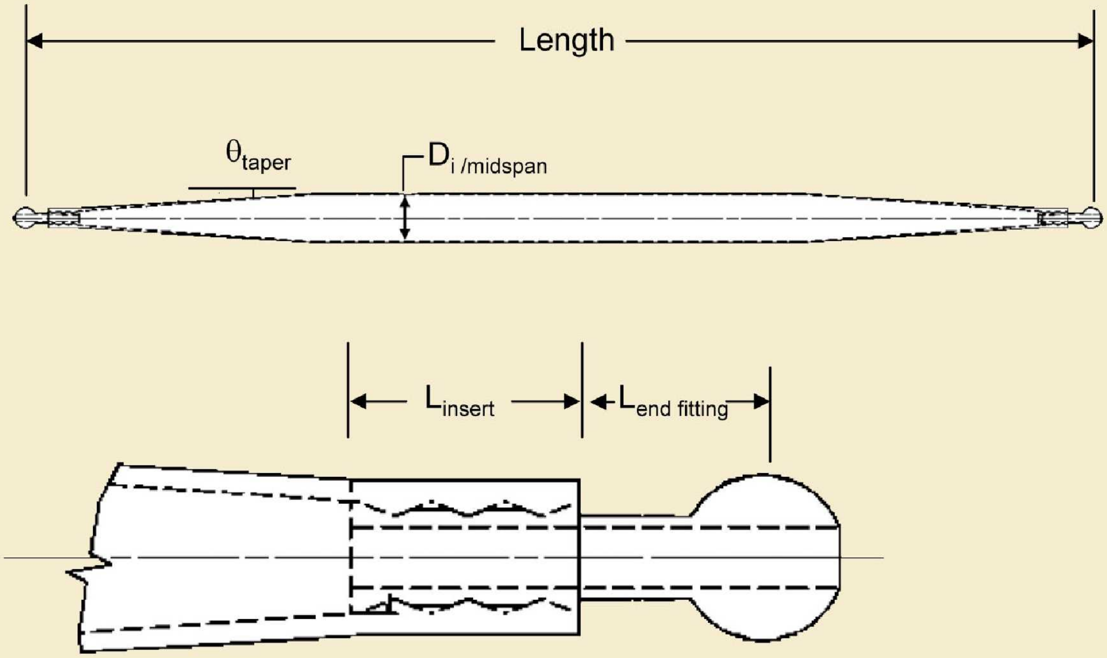

Dimensions

	44k	110k
Length [in]	135	127
$L_{end\ fitting}$ [in]	3	4
L_{insert} [in]	3.272	4.061
$D_{i\ /\ midspan}$ [in]	6	6.5
# 0° plies	11	18
# 90° plies	4	6
t 0° plies [in]	0.00711	
t 90° plies [in]	0.0055	
θ_{taper}	4°	

149764-017

Figure 2.3.4-1. Strut Parameters

Straight Segments (Midspan)

The straight section in the middle of the strut is a simple layup of 0-deg and 90-deg plies. The diameter of the mandrel is 6.0 inches at midspan, and it is wrapped with 11 0-deg plies and 4 90-deg plies. Each 0-deg ply is 0.00711 inch thick; each 90-deg ply is 0.0055 inch thick

$r_{i\ /\ midspan} = 6 / 2 = 3$ in

$t_{0\ /\ midspan} = 11 * 0.00711 = 0.07821$ in

$t_{90} = 4 * 0.0055 = 0.022$ in

$t_{lam\ /\ midspan} = t_{0\ /\ midspan} + t_{90} = 0.07821 + 0.022 = 0.10021$ in

$r_{o\ /\ midspan} = r_{i\ /\ midspan} + t_{lam\ /\ midspan} = 3 + 0.10021 = 3.10021$ in

The modulus of elasticity of the laminate was approximated using the moduli and relative areas of 0-deg and 90-deg plies.

$E_{longitudinal} = 21{,}000{,}000$ psi

$E_{transverse} = 1{,}100{,}000$ psi

$E_{lam / midspan} = (t_{0 / midspan} / t_{lam / midspan}) * E_{longitudinal} + (t_{90} / t_{lam / midspan}) * E_{transverse}$

$E_{lam / midspan} = (0.07821 / 0.10021) * 21{,}000{,}000 + (0.022 / 0.10021) * 1{,}100{,}000 = 16{,}631{,}175$ psi

The moment of inertia of the midspan section is

$I = \pi/4\ (r_{o / midspan}{}^4 - r_{i / midspan}{}^4)$

$I = \pi/4\ [(3.10021)^4 - (3.0)^4] = 8.9356\ in^4$

$EI = 148{,}609{,}101\ lb\text{-}in^2$

Insert Segments

The insert section of the strut was analyzed considering only the composite strut body plies – the titanium insert and the overwrap plies are ignored.

The diameter of the bulb (D_{bulb}) on the insert was taken as the inner diameter of the composite

$r_{i / insert} = 1.772 / 2 = 0.886$ in

The thickness of the 0-deg plies on the insert can be determined from the fact that the cross sectional area of the 0-deg plies is constant over the length of the strut. The diameter and thickness of the 0-deg plies is known at the midspan.

$A_0 = \pi\ (r_{i / midspan} + t_{0 / midspan})^2 - r_{i / midspan}{}^2] \quad = \pi * [(3 + 0.07821)^2 - 3^2] = 1.493\ in^2$

$t_{0 / insert} = ([(A_0 / \pi) + r_{i / insert}{}^2]^{1/2} \ - r_{i / insert}$

$t_{0 / insert} = ([(1.493 / \pi) + 0.886^2]^{1/2} \ - 0.886 = 0.237$ in

Since the thickness of the 90-deg plies is constant over the length of the strut, the thickness of the laminate at the insert can be determined.

$t_{lam / insert} = t_{0 / insert} + t_{90} = 0.237 + 0.022 = 0.259$ in

The outer radius of the laminate at the insert is

$r_{o / insert} = r_{i / insert} + t_{lam / insert}$

$r_{o / insert} = 0.886 + 0.259 = 1.145$ in

The modulus of elasticity of the laminate is approximated using the moduli and relative areas of 0-deg and 90-deg plies.

$E_{lam / insert} = (t_{0 / insert} / t_{lam / insert}) * E_{longitudinal} + (t_{90} / t_{lam / insert}) * E_{transverse}$

$E_{lam / insert} = (0.237 / 0.259) * 21{,}000{,}000 + (0.022 / 0.259) * 1{,}100{,}000 = 19{,}307{,}452$ psi

The moment of inertia of the composite at the insert is

$I = \pi/4\ (r_{o / insert}{}^4 - r_{i / insert}{}^4)$

$I = \pi/4\ [(1.145)^4 - (0.886)^4] = 0.8644\ in^4$

$EI = 16{,}688{,}733\ lb\text{-}in^2$

Taper Segments

The inner radius of the taper section of the strut and the modulus of elasticity were interpolated between the values at the insert and at the straight section. The ply thicknesses and outer radius were then calculated using the same groundrules mentioned previously – the cross-sectional area of the 0-deg plies is constant over the length of the strut, and the thickness of the 90-deg plies is constant over the length of the strut. Moments of inertia were then calculated from these thicknesses.

The taper section begins after the end fitting and insert

$x_{0\,/\,taper} = L_{end\ fitting} + L_{insert} = 3.000 + 3.272 = 6.272$ in

The taper angle is 4°; the length of the taper is given by

$L_{taper} = (r_{i\,/\,midspan} - r_{i\,/\,insert}) / \tan \theta_{taper}$

$L_{taper} = (3 - 0.886) / \tan 4° = 30.232$ in

The inner radius of the taper at station x is

$r_{i\,/\,taper} = r_{i\,/\,insert} + \tan(\theta_{taper}) * (x - x_{0\,/\,taper})$

$r_{i\,/\,taper} = 0.886 + \tan(4°) * (x - 6.272)$

The corresponding outer radius is

$r_{o\,/\,taper} = t_{90} + [(A_0 / \pi) + r_{i\,/\,taper}^2]^{½}$

$r_{o\,/\,taper} = 0.022 + [(1.493 / \pi) + r_{i\,/\,taper}^2]^{½}$

The modulus of elasticity at station x is

$E_{lam\,/\,taper} = E_{lam\,/\,midspan} - [(x - x_{0\,/\,taper}) / L_{taper}] * (E_{lam\,/\,insert} - E_{lam\,/\,midspan})$

$E_{lam\,/\,taper} = 16{,}631{,}175 - [(x - 6.272) / 30.232] * (19{,}307{,}452 - 16{,}631{,}175)$

$E_{lam\,/\,taper} = 16{,}631{,}175 - 88524.64\ (x - 6.272)$

And the moment of inertia is

$I = \pi/4\ (r_{o\,/\,taper}^4 - r_{i\,/\,taper}^4)$

The values of E, I, and (EI) are tabulated for each segment of the strut in Figure 2.3.4.1-1.

Node	Description	Material	Sta	E [psi]	I [in^4]	EI [lb-in^2]
1	end fitting	metal	0	16000000	0.10730	1,716,766
2	end fitting	metal	1.5	16000000	0.10730	1,716,766
3	ftg/insert	metal	3	16000000	0.10730	1,716,766
3	ftg/insert	composite	3	19307452	0.86437	16,688,733
4	insert	composite	4.5	19307452	0.86437	16,688,733
5	insert	composite	6	19307452	0.86437	16,688,733
6	taper	composite	7.5	19,198,742	1.00301	19,256,453
7	taper	composite	9	19,065,954	1.19148	22,716,724
8	taper	composite	10.5	18,933,165	1.40142	26,533,372
9	taper	composite	12	18,800,376	1.63330	30,706,566
10	taper	composite	13.5	18,667,587	1.88757	35,236,292
11	taper	composite	15	18,534,799	2.16470	40,122,339
12	taper	composite	16.5	18,402,010	2.46518	45,364,279
13	taper	composite	18	18,269,221	2.78947	50,961,462
14	taper	composite	19.5	18,136,433	3.13805	56,913,005
15	taper	composite	21	18,003,644	3.51139	63,217,787
16	taper	composite	22.5	17,870,855	3.90997	69,874,449

Node	Description	Material	Sta	E [psi]	I [in^4]	EI [$lb\text{-}in^2$]
17	taper	composite	24	17,738,067	4.33426	76,881,383
18	taper	composite	25.5	17,605,278	4.78474	84,236,739
19	taper	composite	27	17,472,489	5.26190	91,938,418
20	taper	composite	28.5	17,339,700	5.76619	99,984,071
21	taper	composite	30	17,206,912	6.29811	108,371,101
22	taper	composite	31.5	17,074,123	6.85814	117,096,657
23	taper	composite	33	16,941,334	7.44674	126,157,639
24	taper	composite	34.5	16,808,546	8.06439	135,550,695
25	taper	composite	36	16,675,757	8.71158	145,272,220
26	straight	composite	37.5	16,631,175	8.93557	148,609,101
27	straight	composite	39	16,631,175	8.93557	148,609,101
28	straight	composite	40.5	16,631,175	8.93557	148,609,101
29	straight	composite	42	16,631,175	8.93557	148,609,101
30	straight	composite	43.5	16,631,175	8.93557	148,609,101
31	straight	composite	45	16,631,175	8.93557	148,609,101
32	straight	composite	46.5	16,631,175	8.93557	148,609,101
33	straight	composite	48	16,631,175	8.93557	148,609,101
34	straight	composite	49.5	16,631,175	8.93557	148,609,101
35	straight	composite	51	16,631,175	8.93557	148,609,101
36	straight	composite	52.5	16,631,175	8.93557	148,609,101
37	straight	composite	54	16,631,175	8.93557	148,609,101
38	straight	composite	55.5	16,631,175	8.93557	148,609,101
39	straight	composite	57	16,631,175	8.93557	148,609,101
40	straight	composite	58.5	16,631,175	8.93557	148,609,101
41	straight	composite	60	16,631,175	8.93557	148,609,101
42	straight	composite	61.5	16,631,175	8.93557	148,609,101
43	straight	composite	63	16,631,175	8.93557	148,609,101
44	straight	composite	64.5	16,631,175	8.93557	148,609,101
45	straight	composite	66	16,631,175	8.93557	148,609,101
46	straight	MIDSPAN	67.5	16,631,175	8.93557	148,609,101
47	straight	composite	69	16,631,175	8.93557	148,609,101
48	straight	composite	70.5	16,631,175	8.93557	148,609,101
49	straight	composite	72	16,631,175	8.93557	148,609,101
50	straight	composite	73.5	16,631,175	8.93557	148,609,101
51	straight	composite	75	16,631,175	8.93557	148,609,101
52	straight	composite	76.5	16,631,175	8.93557	148,609,101
53	straight	composite	78	16,631,175	8.93557	148,609,101
54	straight	composite	79.5	16,631,175	8.93557	148,609,101
55	straight	composite	81	16,631,175	8.93557	148,609,101
56	straight	composite	82.5	16,631,175	8.93557	148,609,101
57	straight	composite	84	16,631,175	8.93557	148,609,101
58	straight	composite	85.5	16,631,175	8.93557	148,609,101
59	straight	composite	87	16,631,175	8.93557	148,609,101
60	straight	composite	88.5	16,631,175	8.93557	148,609,101
61	straight	composite	90	16,631,175	8.93557	148,609,101
62	straight	composite	91.5	16,631,175	8.93557	148,609,101
63	straight	composite	93	16,631,175	8.93557	148,609,101
64	straight	composite	94.5	16,631,175	8.93557	148,609,101
65	straight	composite	96	16,631,175	8.93557	148,609,101
66	straight	composite	97.5	16,631,175	8.93557	148,609,101
67	taper	composite	99	16,675,757	8.71158	145,272,220
68	taper	composite	100.5	16,808,546	8.06439	135,550,695
69	taper	composite	102	16,941,334	7.44674	126,157,639
70	taper	composite	103.5	17,074,123	6.85814	117,096,657

Node	Description	Material	Sta	E [psi]	I [in^4]	EI [$lb\text{-}in^2$]
71	taper	composite	105	17,206,912	6.29811	108,371,101
72	taper	composite	106.5	17,339,700	5.76619	99,984,071
73	taper	composite	108	17,472,489	5.26190	91,938,418
74	taper	composite	109.5	17,605,278	4.78474	84,236,739
75	taper	composite	111	17,738,067	4.33426	76,881,383
76	taper	composite	112.5	17,870,855	3.90997	69,874,449
77	taper	composite	114	18,003,644	3.51139	63,217,787
78	taper	composite	115.5	18,136,433	3.13805	56,913,005
79	taper	composite	117	18,269,221	2.78947	50,961,462
80	taper	composite	118.5	18,402,010	2.46518	45,364,279
81	taper	composite	120	18,534,799	2.16470	40,122,339
82	taper	composite	121.5	18,667,587	1.88757	35,236,292
83	taper	composite	123	18,800,376	1.63330	30,706,566
84	taper	composite	124.5	18,933,165	1.40142	26,533,372
85	taper	composite	126	19,065,954	1.19148	22,716,724
86	taper	composite	127.5	19,198,742	1.00301	19,256,453
87	insert	composite	129	19307452	0.86437	16,688,733
88	insert	composite	130.5	19307452	0.86437	16,688,733
89	ftg/insert	composite	132	19307452	0.86437	16,688,733
89	ftg/insert	metal	132	16000000	0.10730	1,716,766
90	end fitting	metal	133.5	16000000	0.10730	1,716,766
91	end fitting	metal	135	16000000	0.10730	1,716,766

Figure 2.3.4.1-1. 44K Strut Properties for Newmark Buckling Analysis

The Newmark buckling analysis was performed on the strut using the properties at each segment, using the procedure documented in the Boeing Design Manual, BDM-6238.

Step 1: An initial deflection is assumed for each node. To facilitate quicker convergence, a parabolic deflection pattern was used for the initial condition:

$$\delta_n = -4[(x_n / L_{strut})^2 - (x_n / L_{strut})]$$

Step 2: The moment is calculated at each node

$$M_n = P\delta_n$$

Step 3: α_n is calculated at each node

$$\alpha_n = -\frac{M_n}{E_n I_n}$$

using the values of (EI) tabulated above

Step 4: The concentrated nodal slope values are calculated at each node using the following parabolic fit equations:

$$R_{an} = \frac{h(7\alpha_n + 6\alpha_{n+1} - \alpha_{n+2})}{24}$$

$$R_{bn} = \frac{h(2\alpha_{n-1} + 20\alpha_n + 2\alpha_{n+1})}{24}$$

$$R_{cn} = \frac{h(-\alpha_{n-2} + 6\alpha_{n-1} + 7\alpha_n)}{24}$$

At the far left node of the strut, the concentrated nodal slope value is

$$\overline{\alpha}_1 = R_{a1}$$

At the far right node of the strut, the concentrated nodal slope value is

$\overline{\alpha}_{91} = R_{c91}$

At the discontinuities between the end fitting and strut body,

$\overline{\alpha}_{3} = R_{a3} + R_{c3}$

$\overline{\alpha}_{89} = R_{a89} + R_{c89}$

At all other nodes,

$\overline{\alpha}_{n} = R_{bn}$

Step 5: The slope is calculated as a cumulative sum of the concentrated nodal slope values:

$\text{slope}_1 = \overline{\alpha}_1$

$\text{slope}_n = \text{slope}_{n-1} + \overline{\alpha}_n$

Step 6: Trial deflections are calculated using the slope and segment length:

$y_{t1} = 0$

$y_{tn} = y_{t(n-1)} + h(\text{slope}_{n-1})$

Step 7: Linear correction factors are calculated for the deflections:

$y_{c1} = 0$

$$y_{cn} = \frac{-h(n-1)(\text{right-most value of } y_t)}{L}$$

Step 8: Corrected final deflections are calculated:

$y_{fn} = y_{tn} + y_{cn}$

Step 9: The deflections are normalized to the maximum deflection of the previous iteration:

$$\delta_n = \frac{y_{fn}(\text{maximum deflection from prior iteration (step 1)})}{\text{maximum value of } y_{fn} \text{ from this iteration (step 8)}}$$

Step 10: The buckling load is calculated:

$$P_{cr} = \frac{\sum M_n y_{fn}}{\sum y_{fn}^2}$$

If the buckling load has converged sufficiently (i.e., shows acceptable agreement with the previous iteration), then the iteration is complete. If it has not converged, the deflections from Step 9 are used as the initial deflections (Step 1) in another iteration.

The values calculated from the initial iteration are tabulated in Figure 2.3.4.1-2 as an example.

The buckling load from the first iteration is

$$P_{cr} = \frac{\sum M_n y_{fn}}{\sum y_{fn}^2}$$

$P_{cr} = 744.44 / 0.0116 = 64{,}451$ lb

The iterated buckling loads are presented in Figure 2.3.4.1-3, along with the ultimate load of 61,600 lb.

Node	Sta	δ_n	M_n	α_n	$\bar{\alpha}_n$	Slope	y_{tn}	y_{cn}	y_{fn}	δ_n	$M_n y_{fn}$	y_{fn}^2
1	0	0.0000	0.0	0	-6.436E-06	-6.436E-06	0	0	0	0	0	0
2	1.5	0.0440	44.0	-2.560E-05	-3.833E-05	-4.477E-05	-9.654E-06	0.0008	0.0008	0.0528	0.036	6.58E-07
3	3	0.0869	86.9	-5.063E-05	-3.175E-05	-8.105E-05	-7.680E-05	0.0016	0.0016	0.1019	0.136	2.45E-06
3	3	0.0869	86.9	-5.208E-06	-4.538E-06							
4	4.5	0.1289	128.9	-7.723E-06	-1.158E-05	-9.263E-05	-1.984E-04	0.0025	0.0023	0.1475	0.292	5.12E-06
5	6	0.1699	169.9	-1.018E-05	-1.505E-05	-1.077E-04	-3.373E-04	0.0033	0.0029	0.1919	0.500	8.68E-06
6	7.5	0.2099	209.9	-1.090E-05	-1.627E-05	-1.239E-04	-4.989E-04	0.0041	0.0036	0.2348	0.757	1.30E-05
7	9	0.2489	248.9	-1.096E-05	-1.641E-05	-1.404E-04	-6.848E-04	0.0049	0.0042	0.2762	1.055	1.80E-05
8	10.5	0.2869	286.9	-1.081E-05	-1.620E-05	-1.566E-04	-8.953E-04	0.0057	0.0048	0.3160	1.391	2.35E-05
9	12	0.3240	324.0	-1.055E-05	-1.582E-05	-1.724E-04	-1.130E-03	0.0066	0.0054	0.3541	1.761	2.95E-05
10	13.5	0.3600	360.0	-1.022E-05	-1.532E-05	-1.877E-04	-1.389E-03	0.0074	0.0060	0.3907	2.159	3.60E-05
11	15	0.3951	395.1	-9.846E-06	-1.477E-05	-2.025E-04	-1.670E-03	0.0082	0.0065	0.4259	2.582	4.27E-05
12	16.5	0.4291	429.1	-9.460E-06	-1.419E-05	-2.167E-04	-1.974E-03	0.0090	0.0071	0.4595	3.027	4.98E-05
13	18	0.4622	462.2	-9.070E-06	-1.361E-05	-2.303E-04	-2.299E-03	0.0098	0.0075	0.4918	3.489	5.70E-05
14	19.5	0.4943	494.3	-8.686E-06	-1.303E-05	-2.433E-04	-2.644E-03	0.0107	0.0080	0.5228	3.967	6.44E-05
15	21	0.5254	525.4	-8.311E-06	-1.247E-05	-2.558E-04	-3.009E-03	0.0115	0.0085	0.5525	4.456	7.19E-05
16	22.5	0.5556	555.6	-7.951E-06	-1.193E-05	-2.677E-04	-3.393E-03	0.0123	0.0089	0.5810	4.954	7.95E-05
17	24	0.5847	584.7	-7.605E-06	-1.141E-05	-2.791E-04	-3.794E-03	0.0131	0.0093	0.6083	5.459	8.72E-05
18	25.5	0.6128	612.8	-7.275E-06	-1.091E-05	-2.900E-04	-4.213E-03	0.0140	0.0097	0.6345	5.968	9.48E-05
19	27	0.6400	640.0	-6.961E-06	-1.044E-05	-3.005E-04	-4.648E-03	0.0148	0.0101	0.6596	6.479	1.02E-04
20	28.5	0.6662	666.2	-6.663E-06	-9.996E-06	-3.105E-04	-5.099E-03	0.0156	0.0105	0.6837	6.991	1.10E-04
21	30	0.6914	691.4	-6.380E-06	-9.571E-06	-3.200E-04	-5.564E-03	0.0164	0.0108	0.7068	7.501	1.18E-04
22	31.5	0.7156	715.6	-6.111E-06	-9.168E-06	-3.292E-04	-6.045E-03	0.0172	0.0112	0.7290	8.007	1.25E-04
23	33	0.7388	738.8	-5.856E-06	-8.785E-06	-3.380E-04	-6.538E-03	0.0181	0.0115	0.7503	8.508	1.33E-04
24	34.5	0.7610	761.0	-5.614E-06	-8.423E-06	-3.464E-04	-7.045E-03	0.0189	0.0118	0.7708	9.003	1.40E-04
25	36	0.7822	782.2	-5.385E-06	-8.107E-06	-3.545E-04	-7.565E-03	0.0197	0.0121	0.7904	9.489	1.47E-04
26	37.5	0.8025	802.5	-5.400E-06	-8.114E-06	-3.626E-04	-8.097E-03	0.0205	0.0124	0.8092	9.967	1.54E-04
27	39	0.8217	821.7	-5.529E-06	-8.293E-06	-3.709E-04	-8.641E-03	0.0213	0.0127	0.8272	10.434	1.61E-04
28	40.5	0.8400	840.0	-5.652E-06	-8.478E-06	-3.794E-04	-9.197E-03	0.0222	0.0130	0.8445	10.888	1.68E-04
29	42	0.8573	857.3	-5.769E-06	-8.652E-06	-3.880E-04	-9.766E-03	0.0230	0.0132	0.8609	11.327	1.75E-04
30	43.5	0.8736	873.6	-5.878E-06	-8.817E-06	-3.969E-04	-1.035E-02	0.0238	0.0135	0.8764	11.751	1.81E-04
31	45	0.8889	888.9	-5.981E-06	-8.971E-06	-4.058E-04	-1.094E-02	0.0246	0.0137	0.8911	12.157	1.87E-04
32	46.5	0.9032	903.2	-6.078E-06	-9.116E-06	-4.149E-04	-1.155E-02	0.0254	0.0139	0.9049	12.545	1.93E-04
33	48	0.9165	916.5	-6.167E-06	-9.250E-06	-4.242E-04	-1.217E-02	0.0263	0.0141	0.9178	12.911	1.98E-04
34	49.5	0.9289	928.9	-6.251E-06	-9.375E-06	-4.336E-04	-1.281E-02	0.0271	0.0143	0.9298	13.257	2.04E-04
35	51	0.9402	940.2	-6.327E-06	-9.490E-06	-4.431E-04	-1.346E-02	0.0279	0.0144	0.9409	13.579	2.09E-04
36	52.5	0.9506	950.6	-6.397E-06	-9.594E-06	-4.527E-04	-1.413E-02	0.0287	0.0146	0.9511	13.877	2.13E-04

Node	Sta	δ_n	M_n	α_n	$\overline{\alpha}_n$	Slope	y_{tn}	y_{cn}	y_{fn}	δ_n	$M_n y_{fn}$	y_{fn}^2
37	54	0.9600	960.0	-6.460E-06	-9.689E-06	-4.623E-04	-1.480E-02	0.0295	0.0147	0.9603	14.150	2.17E-04
38	55.5	0.9684	968.4	-6.516E-06	-9.774E-06	-4.721E-04	-1.550E-02	0.0304	0.0149	0.9686	14.397	2.21E-04
39	57	0.9758	975.8	-6.566E-06	-9.849E-06	-4.820E-04	-1.621E-02	0.0312	0.0150	0.9759	14.617	2.24E-04
40	58.5	0.9822	982.2	-6.609E-06	-9.913E-06	-4.919E-04	-1.693E-02	0.0320	0.0151	0.9823	14.809	2.27E-04
41	60	0.9877	987.7	-6.646E-06	-9.968E-06	-5.018E-04	-1.767E-02	0.0328	0.0152	0.9877	14.973	2.30E-04
42	61.5	0.9921	992.1	-6.676E-06	-1.001E-05	-5.119E-04	-1.842E-02	0.0336	0.0152	0.9921	15.107	2.32E-04
43	63	0.9956	995.6	-6.699E-06	-1.005E-05	-5.219E-04	-1.919E-02	0.0345	0.0153	0.9956	15.213	2.33E-04
44	64.5	0.9980	998.0	-6.716E-06	-1.007E-05	-5.320E-04	-1.997E-02	0.0353	0.0153	0.9980	15.288	2.35E-04
45	66	0.9995	999.5	-6.726E-06	-1.009E-05	-5.421E-04	-2.077E-02	0.0361	0.0153	0.9995	15.334	2.35E-04
46	67.5	1.0000	1000.0	-6.729E-06	-1.009E-05	-5.522E-04	-2.158E-02	0.0369	0.0153	1.0000	15.349	2.36E-04
47	69	0.9995	999.5	-6.726E-06	-1.009E-05	-5.623E-04	-2.241E-02	0.0378	0.0153	0.9995	15.334	2.35E-04
48	70.5	0.9980	998.0	-6.716E-06	-1.007E-05	-5.723E-04	-2.325E-02	0.0386	0.0153	0.9980	15.288	2.35E-04
49	72	0.9956	995.6	-6.699E-06	-1.005E-05	-5.824E-04	-2.411E-02	0.0394	0.0153	0.9956	15.213	2.33E-04
50	73.5	0.9921	992.1	-6.676E-06	-1.001E-05	-5.924E-04	-2.499E-02	0.0402	0.0152	0.9921	15.107	2.32E-04
51	75	0.9877	987.7	-6.646E-06	-9.968E-06	-6.024E-04	-2.587E-02	0.0410	0.0152	0.9877	14.973	2.30E-04
52	76.5	0.9822	982.2	-6.609E-06	-9.913E-06	-6.123E-04	-2.678E-02	0.0419	0.0151	0.9823	14.809	2.27E-04
53	78	0.9758	975.8	-6.566E-06	-9.849E-06	-6.221E-04	-2.770E-02	0.0427	0.0150	0.9759	14.617	2.24E-04
54	79.5	0.9684	968.4	-6.516E-06	-9.774E-06	-6.319E-04	-2.863E-02	0.0435	0.0149	0.9686	14.397	2.21E-04
55	81	0.9600	960.0	-6.460E-06	-9.689E-06	-6.416E-04	-2.958E-02	0.0443	0.0147	0.9603	14.150	2.17E-04
56	82.5	0.9506	950.6	-6.397E-06	-9.594E-06	-6.512E-04	-3.054E-02	0.0451	0.0146	0.9511	13.877	2.13E-04
57	84	0.9402	940.2	-6.327E-06	-9.490E-06	-6.607E-04	-3.152E-02	0.0460	0.0144	0.9409	13.579	2.09E-04
58	85.5	0.9289	928.9	-6.251E-06	-9.375E-06	-6.700E-04	-3.251E-02	0.0468	0.0143	0.9298	13.257	2.04E-04
59	87	0.9165	916.5	-6.167E-06	-9.250E-06	-6.793E-04	-3.351E-02	0.0476	0.0141	0.9178	12.911	1.98E-04
60	88.5	0.9032	903.2	-6.078E-06	-9.116E-06	-6.884E-04	-3.453E-02	0.0484	0.0139	0.9049	12.545	1.93E-04
61	90	0.8889	888.9	-5.981E-06	-8.971E-06	-6.974E-04	-3.556E-02	0.0492	0.0137	0.8911	12.157	1.87E-04
62	91.5	0.8736	873.6	-5.878E-06	-8.817E-06	-7.062E-04	-3.661E-02	0.0501	0.0135	0.8764	11.751	1.81E-04
63	93	0.8573	857.3	-5.769E-06	-8.652E-06	-7.148E-04	-3.767E-02	0.0509	0.0132	0.8609	11.327	1.75E-04
64	94.5	0.8400	840.0	-5.652E-06	-8.478E-06	-7.233E-04	-3.874E-02	0.0517	0.0130	0.8445	10.888	1.68E-04
65	96	0.8217	821.7	-5.529E-06	-8.293E-06	-7.316E-04	-3.983E-02	0.0525	0.0127	0.8272	10.434	1.61E-04
66	97.5	0.8025	802.5	-5.400E-06	-8.114E-06	-7.397E-04	-4.092E-02	0.0533	0.0124	0.8092	9.967	1.54E-04
67	99	0.7822	782.2	-5.385E-06	-8.107E-06	-7.478E-04	-4.203E-02	0.0542	0.0121	0.7904	9.489	1.47E-04
68	100.5	0.7610	761.0	-5.614E-06	-8.423E-06	-7.563E-04	-4.316E-02	0.0550	0.0118	0.7708	9.003	1.40E-04
69	102	0.7388	738.8	-5.856E-06	-8.785E-06	-7.650E-04	-4.429E-02	0.0558	0.0115	0.7503	8.508	1.33E-04
70	103.5	0.7156	715.6	-6.111E-06	-9.168E-06	-7.742E-04	-4.544E-02	0.0566	0.0112	0.7290	8.007	1.25E-04
71	105	0.6914	691.4	-6.380E-06	-9.571E-06	-7.838E-04	-4.660E-02	0.0574	0.0108	0.7068	7.501	1.18E-04
72	106.5	0.6662	666.2	-6.663E-06	-9.996E-06	-7.938E-04	-4.777E-02	0.0583	0.0105	0.6837	6.991	1.10E-04
73	108	0.6400	640.0	-6.961E-06	-1.044E-05	-8.042E-04	-4.896E-02	0.0591	0.0101	0.6596	6.479	1.02E-04
74	109.5	0.6128	612.8	-7.275E-06	-1.091E-05	-8.151E-04	-5.017E-02	0.0599	0.0097	0.6345	5.968	9.48E-05

Node	Sta	δ_n	M_n	α_n	$\overline{\alpha}_n$	Slope	y_{tn}	y_{cn}	y_{fn}	δ_n	$M_n y_{fn}$	y_{fn}^2
75	111	0.5847	584.7	-7.605E-06	-1.141E-05	-8.265E-04	-5.139E-02	0.0607	0.0093	0.6083	5.459	8.72E-05
76	112.5	0.5556	555.6	-7.951E-06	-1.193E-05	-8.385E-04	-5.263E-02	0.0616	0.0089	0.5810	4.954	7.95E-05
77	114	0.5254	525.4	-8.311E-06	-1.247E-05	-8.509E-04	-5.389E-02	0.0624	0.0085	0.5525	4.456	7.19E-05
78	115.5	0.4943	494.3	-8.686E-06	-1.303E-05	-8.640E-04	-5.517E-02	0.0632	0.0080	0.5228	3.967	6.44E-05
79	117	0.4622	462.2	-9.070E-06	-1.361E-05	-8.776E-04	-5.646E-02	0.0640	0.0075	0.4918	3.489	5.70E-05
80	118.5	0.4291	429.1	-9.460E-06	-1.419E-05	-8.918E-04	-5.778E-02	0.0648	0.0071	0.4595	3.027	4.98E-05
81	120	0.3951	395.1	-9.846E-06	-1.477E-05	-9.065E-04	-5.912E-02	0.0657	0.0065	0.4259	2.582	4.27E-05
82	121.5	0.3600	360.0	-1.022E-05	-1.532E-05	-9.219E-04	-6.048E-02	0.0665	0.0060	0.3907	2.159	3.60E-05
83	123	0.3240	324.0	-1.055E-05	-1.582E-05	-9.377E-04	-6.186E-02	0.0673	0.0054	0.3541	1.761	2.95E-05
84	124.5	0.2869	286.9	-1.081E-05	-1.620E-05	-9.539E-04	-6.327E-02	0.0681	0.0048	0.3160	1.391	2.35E-05
85	126	0.2489	248.9	-1.096E-05	-1.641E-05	-9.703E-04	-6.470E-02	0.0689	0.0042	0.2762	1.055	1.80E-05
86	127.5	0.2099	209.9	-1.090E-05	-1.627E-05	-9.866E-04	-6.615E-02	0.0698	0.0036	0.2348	0.757	1.30E-05
87	129	0.1699	169.9	-1.018E-05	-1.505E-05	-1.002E-03	-6.763E-02	0.0706	0.0029	0.1919	0.500	8.68E-06
88	130.5	0.1289	128.9	-7.723E-06	-1.158E-05	-1.013E-03	-6.914E-02	0.0714	0.0023	0.1475	0.292	5.12E-06
89	132	0.0869	86.9	-5.208E-06	-4.538E-06	-1.049E-03	-7.065E-02	0.0722	0.0016	0.1019	0.136	2.45E-06
89	132	0.0869	86.9	-5.063E-05	-3.175E-05							
90	133.5	0.0440	44.0	-2.560E-05	-3.833E-05	-1.088E-03	-7.223E-02	0.0730	0.0008	0.0528	0.036	6.58E-07
91	135	0.0000	0.0	0.000E+00	-6.436E-06	-1.094E-03	-7.386E-02	0.0739	0	0	0	0
										Sum:	744.44	0.0116

Figure 2.3.4.1-2. Newmark Buckling Analysis Results of 44K Strut

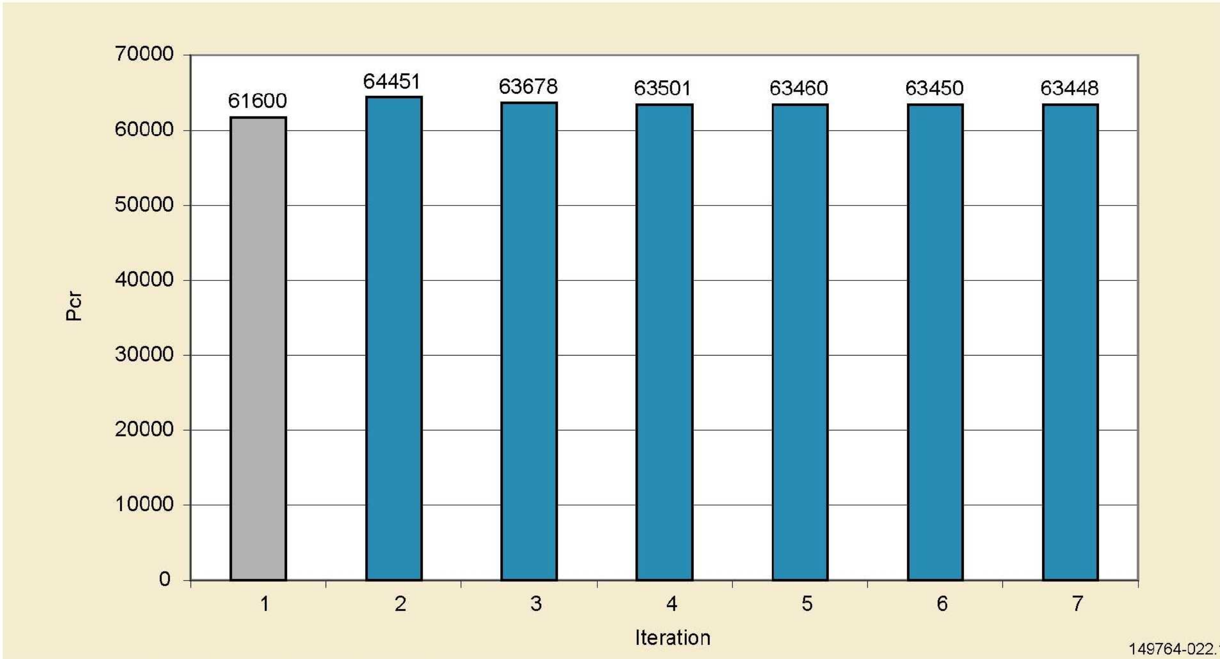

Figure 2.3.4.1-3. Iterated Buckling Loads of 44K Strut

2.3.4.2 110K Strut

The 110K strut is divided into 64 axial segments, corresponding to a segment length of 1.984 inches. Although this segment length divides evenly into the overall strut length, the end fitting length was adjusted from 4 inches to 3.969 inches in the analysis to ensure a node at the transition between the end fitting and strut body. The analysis approach is the same as that used for the 44K strut.

End Fitting Segments

E = 160,000,000 psi

$I = \pi/4\ [(2.145 / 2)^4 - (1.625 / 2)^4] = 0.6969\ in^4$

$EI = 11,149,929\ lb\text{-}in^2$

Straight Segments (Midspan)

The diameter of the mandrel is 6.5 inches at the midspan, and it is wrapped with 18 0-deg plies and 6 90-deg plies.

$r_{i\,/\,midspan} = 6.5 / 2 = 3.25$ in

$t_{0\,/\,midspan} = 18 * 0.00711 = 0.12798$ in

$t_{90} = 6 * 0.0055 = 0.033$ in

$t_{lam\,/\,midspan} = t_{0\,/\,midspan} + t_{90} = 0.12798 + 0.033 = 0.1610$ in

$r_{o\,/\,midspan} = r_{i\,/\,midspan} + t_{lam\,/\,midspan} = 3.25 + 0.\ 1610 = 3.411$ in

$E_{lam\,/\,midspan} = (0.\ 12798 / 0.\ 1610) * 21,000,000 + (0.\ 033 / 0.\ 1610) * 1,100,000 = 16,920,611$ psi

$I = \pi/4\ [(3.\ 411)^4 - (3.\ 25)^4] = 18.6939\ in^4$

$EI = 316{,}312{,}119$ lb-in^2

Insert Segments

$r_{i\,/\,insert} = 2.686 / 2 = 1.343$ in

$A_0 = \pi\,(r_{i\,/\,midspan} + t_{0\,/\,midspan})^2 - r_{i\,/\,midspan}{}^2] \quad = \pi * [(3.25 + 0.12798)^2 - 3.25^2] = 2.665$ in^2

$t_{0\,/\,insert} = [(2.665 / \pi) + 1.343^2]^{½} - 1.343 = 0.285$ in

$t_{lam\,/\,insert} = t_{0\,/\,insert} + t_{90} = 0.285 + 0.033 = 0.318$ in

$r_{o\,/\,insert} = 1.343 + 0.318 = 1.661$ in

$E_{lam\,/\,insert} = (0.285 / 0.318) * 21{,}000{,}000 + (0.033 / 0.318) * 1{,}100{,}000 = 18{,}937{,}920$ psi

$I = \pi/4\ [(1.661)^4 - (1.343)^4] = 3.4298$ in^4

$EI = 64{,}954{,}222$ lb-in^2

Taper Segments

$x_{0\,/\,taper} = L_{end\ fitting} + L_{insert} = 4.061 + 3.969 = 8.030$ in

$L_{taper} = (3.25 - 1.343) / \tan 4° = 27.271$ in

$r_{i\,/\,taper} = 1.343 + \tan(4°) * (x - 8.030)$

$r_{o\,/\,taper} = 0.033 + [(2.665 / \pi) + r_{i\,/\,taper}{}^2]^{½}$

$E_{lam\,/\,taper} = 18{,}937{,}920 - [(x - 8.030) / 27.271] * (18{,}937{,}920 - 16{,}920{,}611)$

$E_{lam\,/\,taper} = 18{,}937{,}920 - 73972.68\ (x - 8.030)$

$I = \pi/4\ (r_{o\,/\,taper}{}^4 - r_{i\,/\,taper}{}^4)$

The values of E, I, and (EI) are tabulated for each segment of the strut in Figure 2.3.4.2-1. The Newmark buckling analysis is performed using the procedure described in the section for the 44k strut. The values calculated from the initial iteration are tabulated in Figure 2.3.4.2-2 as an example.

Node	Description	Material	Sta	E [psi]	I [in^4]	EI [lb-in^2]
1	end fitting	metal	0.00	16000000	0.69687	11149929
2	end fitting	metal	1.98	16000000	0.69687	11149929
3	ftg /insert	metal	3.97	16000000	0.69687	11149929
3	ftg /insert	composite	3.97	18937920	3.42985	64954222
4	insert	composite	5.95	18937920	3.42985	64954222
5	insert	composite	7.94	18937920	3.42985	64954222
6	taper	composite	9.92	18797956	4.02630	75686269
7	taper	composite	11.91	18651169	4.71967	88027297
8	taper	composite	13.89	18504381	5.48406	101479205
9	taper	composite	15.88	18357593	6.32112	116040554
10	taper	composite	17.86	18210806	7.23247	131709100
11	taper	composite	19.84	18064018	8.21975	148481752
12	taper	composite	21.83	17917231	9.28461	166354540
13	taper	composite	23.81	17770443	10.42870	185322588
14	taper	composite	25.80	17623656	11.65366	205380100
15	taper	composite	27.78	17476868	12.96115	226520347
16	taper	composite	29.77	17330081	14.35283	248735658
17	taper	composite	31.75	17183293	15.83034	272017411
18	taper	composite	33.73	17036506	17.39535	296356032

Node	Description	Material	Sta	E [psi]	I [in^4]	EI [lb-in^2]
19	straight	composite	35.72	16920611	18.69389	316312119
20	straight	composite	37.70	16920611	18.69389	316312119
21	straight	composite	39.69	16920611	18.69389	316312119
22	straight	composite	41.67	16920611	18.69389	316312119
23	straight	composite	43.66	16920611	18.69389	316312119
24	straight	composite	45.64	16920611	18.69389	316312119
25	straight	composite	47.63	16920611	18.69389	316312119
26	straight	composite	49.61	16920611	18.69389	316312119
27	straight	composite	51.59	16920611	18.69389	316312119
28	straight	composite	53.58	16920611	18.69389	316312119
29	straight	composite	55.56	16920611	18.69389	316312119
30	straight	composite	57.55	16920611	18.69389	316312119
31	straight	composite	59.53	16920611	18.69389	316312119
32	straight	composite	61.52	16920611	18.69389	316312119
33	straight	MIDSPAN	63.50	16920611	18.69389	316312119
34	straight	composite	65.48	16920611	18.69389	316312119
35	straight	composite	67.47	16920611	18.69389	316312119
36	straight	composite	69.45	16920611	18.69389	316312119
37	straight	composite	71.44	16920611	18.69389	316312119
38	straight	composite	73.42	16920611	18.69389	316312119
39	straight	composite	75.41	16920611	18.69389	316312119
40	straight	composite	77.39	16920611	18.69389	316312119
41	straight	composite	79.38	16920611	18.69389	316312119
42	straight	composite	81.36	16920611	18.69389	316312119
43	straight	composite	83.34	16920611	18.69389	316312119
44	straight	composite	85.33	16920611	18.69389	316312119
45	straight	composite	87.31	16920611	18.69389	316312119
46	straight	composite	89.30	16920611	18.69389	316312119
47	straight	composite	91.28	16920611	18.69389	316312119
48	taper	composite	93.27	17036506	17.39535	296356032
49	taper	composite	95.25	17183293	15.83034	272017411
50	taper	composite	97.23	17330081	14.35283	248735658
51	taper	composite	99.22	17476868	12.96115	226520347
52	taper	composite	101.20	17623656	11.65366	205380100
53	taper	composite	103.19	17770443	10.42870	185322588
54	taper	composite	105.17	17917231	9.28461	166354540
55	taper	composite	107.16	18064018	8.21975	148481752
56	taper	composite	109.14	18210806	7.23247	131709100
57	taper	composite	111.13	18357593	6.32112	116040554
58	taper	composite	113.11	18504381	5.48406	101479205
59	taper	composite	115.09	18651169	4.71967	88027297
60	taper	composite	117.08	18797956	4.02630	75686269
61	insert	composite	119.06	18937920	3.42985	64954222
62	insert	composite	121.05	18937920	3.42985	64954222
63	ftg/insert	composite	123.03	18937920	3.42985	64954222
63	ftg /insert	metal	123.03	16000000	0.69687	11149929
64	end fitting	metal	125.02	16000000	0.69687	11149929
65	end fitting	metal	127.00	16000000	0.69687	11149929

Figure 2.3.4.2-1. 110K Strut Properties for Newmark Buckling Analysis

Node	Sta	δ_n	M_n	α_n	$\overline{\alpha}_n$	Slope	y_{tn}	y_{cn}	y_{fn}	δ_n	$M_n y_{fn}$	y_{fn}^2
1	0.00	0.0000	0.0	0.000E+00	-1.839E-06	-1.839E-06	0.000E+00	0.0000	0.0000	0.0000	0.000	0.00E+00
2	1.98	0.0615	61.5	-5.518E-06	-1.092E-05	-1.276E-05	-3.650E-06	0.0004	0.0004	0.0662	0.025	1.67E-07
3	3.97	0.1211	121.1	-1.086E-05	-9.023E-06	-2.393E-05	-2.897E-05	0.0008	0.0008	0.1288	0.096	6.33E-07
3	3.97	0.1211	121.1	-1.864E-06	-2.146E-06							
4	5.95	0.1787	178.7	-2.751E-06	-5.455E-06	-2.938E-05	-7.645E-05	0.0012	0.0012	0.1879	0.207	1.35E-06
5	7.94	0.2344	234.4	-3.608E-06	-7.051E-06	-3.643E-05	-1.348E-04	0.0016	0.0015	0.2453	0.355	2.29E-06
6	9.92	0.2881	288.1	-3.806E-06	-7.529E-06	-4.396E-05	-2.071E-04	0.0021	0.0019	0.3003	0.534	3.44E-06
7	11.91	0.3398	339.8	-3.861E-06	-7.649E-06	-5.161E-05	-2.943E-04	0.0025	0.0022	0.3530	0.741	4.75E-06
8	13.89	0.3896	389.6	-3.840E-06	-7.611E-06	-5.922E-05	-3.967E-04	0.0029	0.0025	0.4031	0.970	6.20E-06
9	15.88	0.4375	437.5	-3.770E-06	-7.477E-06	-6.670E-05	-5.142E-04	0.0033	0.0028	0.4509	1.218	7.75E-06
10	17.86	0.4834	483.4	-3.670E-06	-7.280E-06	-7.398E-05	-6.466E-04	0.0037	0.0031	0.4962	1.481	9.39E-06
11	19.84	0.5273	527.3	-3.552E-06	-7.046E-06	-8.103E-05	-7.934E-04	0.0041	0.0033	0.5392	1.756	1.11E-05
12	21.83	0.5693	569.3	-3.422E-06	-6.791E-06	-8.782E-05	-9.542E-04	0.0045	0.0036	0.5799	2.039	1.28E-05
13	23.81	0.6094	609.4	-3.288E-06	-6.525E-06	-9.434E-05	-1.128E-03	0.0049	0.0038	0.6185	2.327	1.46E-05
14	25.80	0.6475	647.5	-3.153E-06	-6.256E-06	-1.006E-04	-1.316E-03	0.0054	0.0040	0.6549	2.619	1.64E-05
15	27.78	0.6836	683.6	-3.018E-06	-5.989E-06	-1.066E-04	-1.515E-03	0.0058	0.0043	0.6894	2.910	1.81E-05
16	29.77	0.7178	717.8	-2.886E-06	-5.727E-06	-1.123E-04	-1.727E-03	0.0062	0.0045	0.7219	3.200	1.99E-05
17	31.75	0.7500	750.0	-2.757E-06	-5.472E-06	-1.178E-04	-1.950E-03	0.0066	0.0046	0.7526	3.485	2.16E-05
18	33.73	0.7803	780.3	-2.633E-06	-5.233E-06	-1.230E-04	-2.183E-03	0.0070	0.0048	0.7815	3.765	2.33E-05
19	35.72	0.8086	808.6	-2.556E-06	-5.099E-06	-1.281E-04	-2.428E-03	0.0074	0.0050	0.8087	4.038	2.49E-05
20	37.70	0.8350	835.0	-2.640E-06	-5.237E-06	-1.334E-04	-2.682E-03	0.0078	0.0052	0.8343	4.302	2.65E-05
21	39.69	0.8594	859.4	-2.717E-06	-5.390E-06	-1.387E-04	-2.946E-03	0.0082	0.0053	0.8583	4.555	2.81E-05
22	41.67	0.8818	881.8	-2.788E-06	-5.531E-06	-1.443E-04	-3.222E-03	0.0087	0.0054	0.8804	4.794	2.96E-05
23	43.66	0.9023	902.3	-2.853E-06	-5.660E-06	-1.499E-04	-3.508E-03	0.0091	0.0056	0.9008	5.020	3.09E-05
24	45.64	0.9209	920.9	-2.911E-06	-5.776E-06	-1.557E-04	-3.806E-03	0.0095	0.0057	0.9194	5.228	3.22E-05
25	47.63	0.9375	937.5	-2.964E-06	-5.880E-06	-1.616E-04	-4.115E-03	0.0099	0.0058	0.9362	5.420	3.34E-05
26	49.61	0.9521	952.1	-3.010E-06	-5.972E-06	-1.676E-04	-4.435E-03	0.0103	0.0059	0.9510	5.592	3.45E-05
27	51.59	0.9648	964.8	-3.050E-06	-6.052E-06	-1.736E-04	-4.768E-03	0.0107	0.0060	0.9639	5.743	3.54E-05
28	53.58	0.9756	975.6	-3.084E-06	-6.119E-06	-1.797E-04	-5.112E-03	0.0111	0.0060	0.9749	5.873	3.62E-05
29	55.56	0.9844	984.4	-3.112E-06	-6.174E-06	-1.859E-04	-5.469E-03	0.0115	0.0061	0.9839	5.981	3.69E-05
30	57.55	0.9912	991.2	-3.134E-06	-6.217E-06	-1.921E-04	-5.838E-03	0.0120	0.0061	0.9909	6.065	3.74E-05
31	59.53	0.9961	996.1	-3.149E-06	-6.248E-06	-1.984E-04	-6.219E-03	0.0124	0.0062	0.9960	6.126	3.78E-05
32	61.52	0.9990	999.0	-3.158E-06	-6.266E-06	-2.046E-04	-6.613E-03	0.0128	0.0062	0.9990	6.163	3.81E-05
33	63.50	1.0000	1000.0	-3.161E-06	-6.272E-06	-2.109E-04	-7.019E-03	0.0132	0.0062	1.0000	6.175	3.81E-05
34	65.48	0.9990	999.0	-3.158E-06	-6.266E-06	-2.172E-04	-7.437E-03	0.0136	0.0062	0.9990	6.163	3.81E-05
35	67.47	0.9961	996.1	-3.149E-06	-6.248E-06	-2.234E-04	-7.868E-03	0.0140	0.0062	0.9960	6.126	3.78E-05
36	69.45	0.9912	991.2	-3.134E-06	-6.217E-06	-2.296E-04	-8.312E-03	0.0144	0.0061	0.9909	6.065	3.74E-05
37	71.44	0.9844	984.4	-3.112E-06	-6.174E-06	-2.358E-04	-8.767E-03	0.0148	0.0061	0.9839	5.981	3.69E-05

Node	Sta	δ_n	M_n	α_n	$\overline{\alpha}_n$	Slope	y_{tn}	y_{cn}	y_{fn}	δ_n	$M_n y_{fn}$	y_{fn}^2
38	73.42	0.9756	975.6	-3.084E-06	-6.119E-06	-2.419E-04	-9.235E-03	0.0153	0.0060	0.9749	5.873	3.62E-05
39	75.41	0.9648	964.8	-3.050E-06	-6.052E-06	-2.480E-04	-9.715E-03	0.0157	0.0060	0.9639	5.743	3.54E-05
40	77.39	0.9521	952.1	-3.010E-06	-5.972E-06	-2.540E-04	-1.021E-02	0.0161	0.0059	0.9510	5.592	3.45E-05
41	79.38	0.9375	937.5	-2.964E-06	-5.880E-06	-2.598E-04	-1.071E-02	0.0165	0.0058	0.9362	5.420	3.34E-05
42	81.36	0.9209	920.9	-2.911E-06	-5.776E-06	-2.656E-04	-1.123E-02	0.0169	0.0057	0.9194	5.228	3.22E-05
43	83.34	0.9023	902.3	-2.853E-06	-5.660E-06	-2.713E-04	-1.175E-02	0.0173	0.0056	0.9008	5.020	3.09E-05
44	85.33	0.8818	881.8	-2.788E-06	-5.531E-06	-2.768E-04	-1.229E-02	0.0177	0.0054	0.8804	4.794	2.96E-05
45	87.31	0.8594	859.4	-2.717E-06	-5.390E-06	-2.822E-04	-1.284E-02	0.0181	0.0053	0.8583	4.555	2.81E-05
46	89.30	0.8350	835.0	-2.640E-06	-5.237E-06	-2.874E-04	-1.340E-02	0.0186	0.0052	0.8343	4.302	2.65E-05
47	91.28	0.8086	808.6	-2.556E-06	-5.099E-06	-2.925E-04	-1.397E-02	0.0190	0.0050	0.8087	4.038	2.49E-05
48	93.27	0.7803	780.3	-2.633E-06	-5.233E-06	-2.978E-04	-1.455E-02	0.0194	0.0048	0.7815	3.765	2.33E-05
49	95.25	0.7500	750.0	-2.757E-06	-5.472E-06	-3.032E-04	-1.514E-02	0.0198	0.0046	0.7526	3.485	2.16E-05
50	97.23	0.7178	717.8	-2.886E-06	-5.727E-06	-3.090E-04	-1.575E-02	0.0202	0.0045	0.7219	3.200	1.99E-05
51	99.22	0.6836	683.6	-3.018E-06	-5.989E-06	-3.150E-04	-1.636E-02	0.0206	0.0043	0.6894	2.910	1.81E-05
52	101.20	0.6475	647.5	-3.153E-06	-6.256E-06	-3.212E-04	-1.698E-02	0.0210	0.0040	0.6549	2.619	1.64E-05
53	103.19	0.6094	609.4	-3.288E-06	-6.525E-06	-3.277E-04	-1.762E-02	0.0214	0.0038	0.6185	2.327	1.46E-05
54	105.17	0.5693	569.3	-3.422E-06	-6.791E-06	-3.345E-04	-1.827E-02	0.0219	0.0036	0.5799	2.039	1.28E-05
55	107.16	0.5273	527.3	-3.552E-06	-7.046E-06	-3.416E-04	-1.893E-02	0.0223	0.0033	0.5392	1.756	1.11E-05
56	109.14	0.4834	483.4	-3.670E-06	-7.280E-06	-3.489E-04	-1.961E-02	0.0227	0.0031	0.4962	1.481	9.39E-06
57	111.13	0.4375	437.5	-3.770E-06	-7.477E-06	-3.563E-04	-2.031E-02	0.0231	0.0028	0.4509	1.218	7.75E-06
58	113.11	0.3896	389.6	-3.840E-06	-7.611E-06	-3.639E-04	-2.101E-02	0.0235	0.0025	0.4031	0.970	6.20E-06
59	115.09	0.3398	339.8	-3.861E-06	-7.649E-06	-3.716E-04	-2.173E-02	0.0239	0.0022	0.3530	0.741	4.75E-06
60	117.08	0.2881	288.1	-3.806E-06	-7.529E-06	-3.791E-04	-2.247E-02	0.0243	0.0019	0.3003	0.534	3.44E-06
61	119.06	0.2344	234.4	-3.608E-06	-7.051E-06	-3.862E-04	-2.322E-02	0.0247	0.0015	0.2453	0.355	2.29E-06
62	121.05	0.1787	178.7	-2.751E-06	-5.455E-06	-3.916E-04	-2.399E-02	0.0252	0.0012	0.1879	0.207	1.35E-06
63	123.03	0.1211	121.1	-1.864E-06	-2.146E-06	-4.028E-04	-2.477E-02	0.0256	0.0008	0.1288	0.096	6.33E-07
63	123.03	0.1211	121.1	-1.086E-05	-9.023E-06							
64	125.02	0.0615	61.5	-5.518E-06	-1.092E-05	-4.137E-04	-2.557E-02	0.0260	0.0004	0.0662	0.025	1.67E-07
65	127.00	0.0000	0.0	0.000E+00	-1.839E-06	-4.156E-04	-2.639E-02	0.0264	0.0000	0.0000	0.000	0.00E+00
										Sum:	211.43	0.00131

Figure 2.3.4.2-2. Newmark Buckling Analysis Results for 110K Strut

The buckling load from the first iteration is

$$P_{cr} = \frac{\sum M_n y_{fn}}{\sum y_{fn}^{2}}$$

$P_{cr} = 211.43 / 0.00131 = 160{,}623$ lb

The iterated buckling loads are presented in Figure 2.3.4.2-3, along with the ultimate load of 154,000 lb.

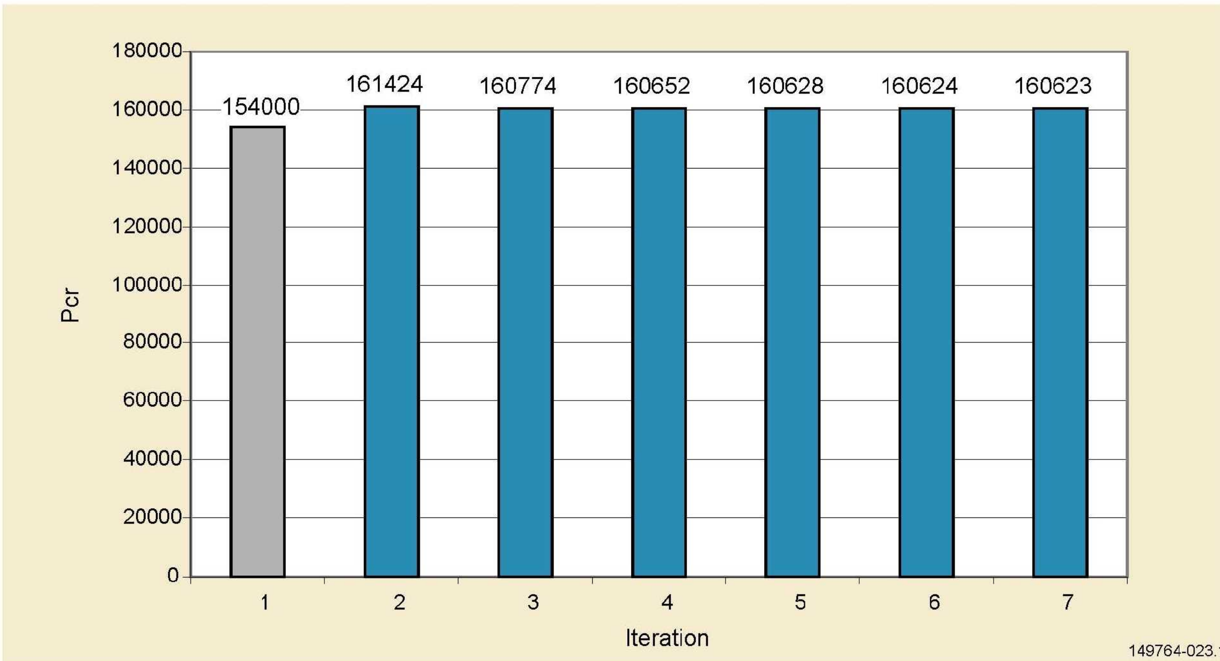

Figure 2.3.4.2-3. Iterated buckling loads of 110K strut

2.3.5 Natural Frequency

The natural frequency of the first mode of a uniform beam with simply supported ends is:

$$f_1 = \frac{9.87}{2\pi}\sqrt{\frac{EIg}{wL^4}}$$

where:

E is the modulus of elasticity

I is the moment of inertia

g is gravitational acceleration (in consistent units)

w is the weight per unit length of the beam

L is the length of the beam (Ref: Roark & Young, 6th edition, Table 36, case 1b)

The Park struts have a significant mass located near the ends in the form of the titanium inserts and end fittings. Since the ends are simply-supported (pinned), these masses will not significantly affect the frequency of the first mode. As an approximation, they will be ignored. Similarly, the taper and overwrap sections will have less effect on the dynamic response than the midspan. Therefore, for this approximation, the midspan properties will be used in the natural frequency equation.

2.3.5.1 44K Strut

The cross-sectional area at the midspan is

$A = \pi\,(r_{o\,/\,midspan}{}^2 - r_{i\,/\,midspan}{}^2) = \pi\,(3.10021^2 - 3^2) = 1.920\ in^2$

and the density of the composite is 0.0555 lb/in^3

The weight per unit length is

$w = \rho A = (0.0555)\,(1.920) = 0.10656\ lb/in$

The natural frequency of the first mode is then

$$f_1 = \frac{9.87}{2\pi}\sqrt{\frac{(16{,}631{,}175)(8.9356)(386.4)}{(0.10656)(135)^4}}$$

$f_1 = 63$ Hz

2.3.5.2 110K Strut

$A = \pi\,(r_{o\,/\,midspan}{}^2 - r_{i\,/\,midspan}{}^2) = \pi\,(3.411^2 - 3.25^2) = 3.369\ in^2$

$w = \rho A = (0.0555)\,(3.369) = 0.18698\ lb/in$

$$f_1 = \frac{9.87}{2\pi}\sqrt{\frac{(16{,}920{,}611)(18.6939)(386.4)}{(0.18698)(127)^4}}$$

$f_1 = 79$ Hz

2.3.6 Compression Stress

The 0-deg plies are assumed to carry the entire axial load; the contribution by the 90-deg plies is neglected.

2.3.6.1 44K Strut

$\sigma_{comp} = P_{ULT} / A_0 = 1.4 * 44{,}000 / 1.493 = 41259$ psi

MS = 191,000 / 41,259 – 1 = 3.63

2.3.6.2 110K Strut

$\sigma_{comp} = P_{ULT} / A_0 = 1.4 * 110{,}000 / 2.665 = 57786$ psi

MS = 191,000 / 57,786 – 1 = 2.31

2.3.7 Crippling/Local Instability

Park applies an empirical equation derived from its own testing to determine the crippling cutoff stress:

$$\sigma_{cr} = \frac{456075}{\sqrt{D_{i\,/\,midspan} / t_{0\,/\,midspan}}}$$

2.3.7.1 44K Strut

$$\sigma_{cr} = \frac{456075}{\sqrt{6/0.07821}} = 52071$$

MS = 52,071 / 41,259 – 1 = 0.26

2.3.7.2 110K Strut

$$\sigma_{cr} = \frac{456075}{\sqrt{6.5/0.12798}} = 63996$$

MS = 63,996 / 57,786 – 1 = 0.11

3.0 MANUFACTURING DEMONSTRATION ARTICLE

3.1 Background

The Shuttle Orbiter program uses aluminum struts (Figure 3.1-1) to replace easily damaged mid-fuselage boron/aluminum struts. However, these aluminum struts add significant weight to the vehicles. In response, Boeing conducted a preliminary development program for lightweight graphite composite struts that would replace the relatively heavy aluminum struts.

Figure 3.1-1. Shuttle Aluminum Replacement Strut Configuration

Boeing and its subcontractor Park Aerospace Structures (previously Nova Composites) conducted design, development, and testing of a lightweight graphite composite replacement strut starting in 2001 (Figure 3.1-2). A preliminary, yet comprehensive, series of development tests included damage tolerance, tension, compression, and extreme environment testing. One concept that was investigated to visualize impact damage was to bond a single ply of fiberglass/epoxy to the outer tube surface. A detailed draft specification was also prepared.

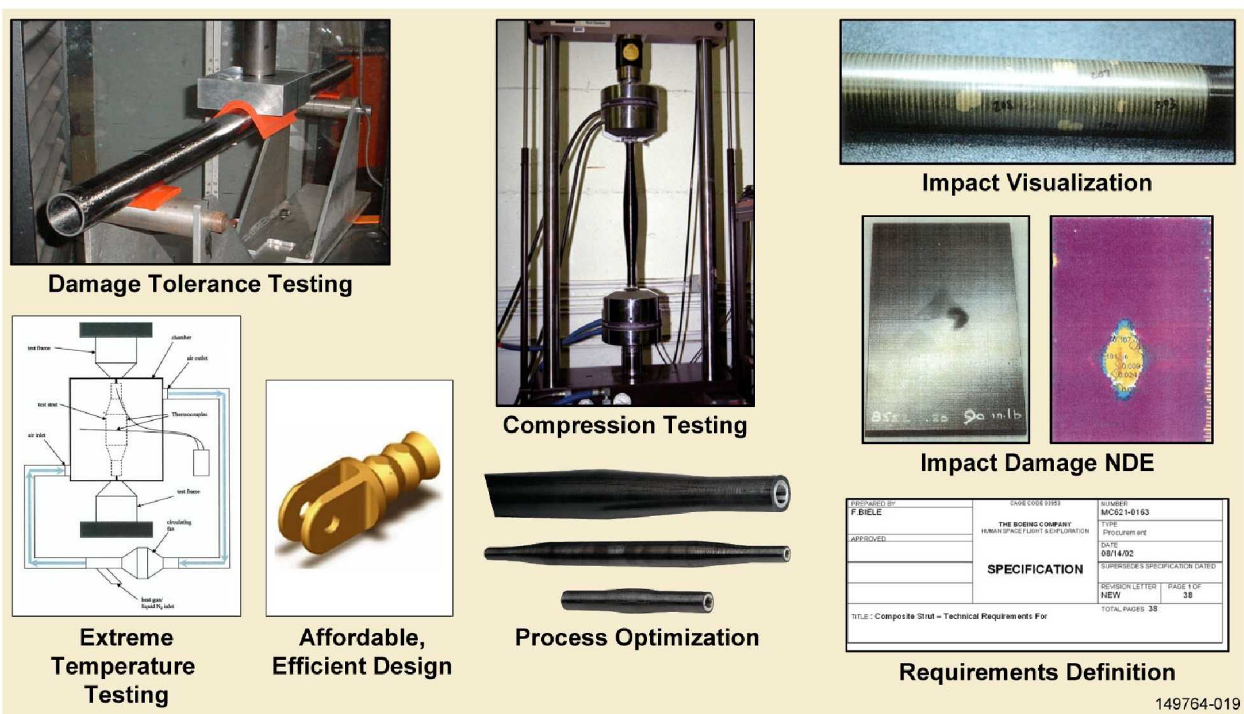

Figure 3.1-2. Shuttle Replacement Strut Development

The objective of the development program was to verify that composite struts could satisfy the design requirements for a human-rated spacecraft while saving weight compared to the aluminum struts. The design requirements included strength, stiffness, and fatigue loading criteria. The composite struts were designed to withstand launch, ascent, on-orbit, descent, and landing loads. Other design goals and guidelines include (1) minimize strut configurations, (2) no overlapping of strut length between configurations, (3) maintain existing strut geometry envelope, (4) minimize cost per pound of weight savings, (5) use existing orbiter attachment hardware, (6) exhibit improved damage tolerance, and (7) reduce replacement cycle time.

A comprehensive set of composite strut designs was developed to replace existing aluminum replacement struts currently on the Shuttle fleet. The end fitting design consists of a clevis that is threaded into a Park insert.

The demo strut fabrication activity provided an understanding of the Park strut fabrication process, and determined the improvements necessary to transition the Park current strut manufacturing process to a fully traceable and repeatable process capable of producing certified space flight hardware.

3.2 Demonstration Strut Design

The strut body is about one half the length of the full-scale analytical struts and has a sufficient number of plies to demonstrate process optimization for a full-scale strut. The selected end fitting features a clevis that is integral with the Park insert (Figures 3.2-1 and 3.2-2). Compared to the adjustable design, advantages of the integral end fitting include (1) approximately the same cost, (2) 33% less weight, and (3) more accurate dimensional control on assembly (holes are drilled in the clevis on assembly). One possible disadvantage is less adjustability.

The representative end fittings are threaded so that can be removed from the inserts. This modification was chosen to preclude changing the Park fabrication process, and to demonstrate the ability to incorporate various end fittings configurations. The 11- ply layup (90,0_4,90,0_4,90) uses IM7/8552 tow and tape prepreg.

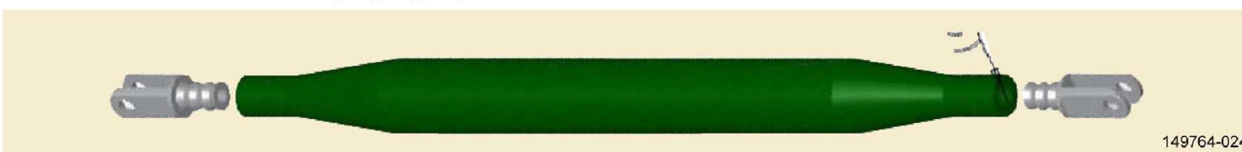

Figure 3.2-1. Selected Composite Strut Body and Integral End Fitting Configuration

Figure 3.2-2. Integral End Fitting Configuration

3.3 Demonstration Strut Fabrication

Each step of the strut manufacturing process is documented in the final report for his task. An outline of the process is included herein. All materials used in these struts are commercially available and nonproprietary.

Figure 3.3-1 summarizes the strut fabrication process. A plaster mandrel is cast onto a steel rod. Machined titanium inserts with center holes are placed on the rod at either end of the plaster mandrel. Collars are placed onto the rod to secure the inserts during strut body fabrication. The strut body is layed up with 90-deg prepreg tow and 0-deg prepreg tape plies onto the plaster mandrel and titanium insert, with intermittent debulks to minimize fiber wrinkling. The plies are also layed onto the insert. The strut body is cured in an autoclave, and the plaster mandrel is washed out. In the improved Boeing process, the end fitting is then final machined from a blank that is an integral part of the insert.

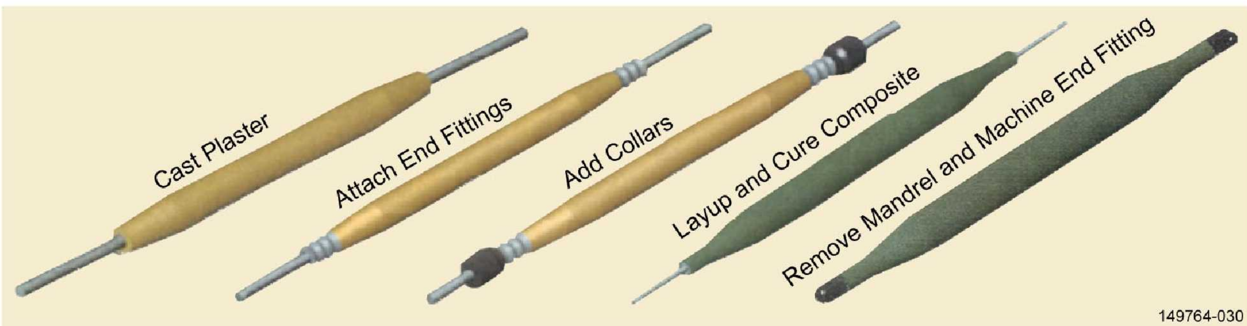

Figure 3.3.1-1. Overview of Strut Fabrication Process

Composite tubular structures are often bagged from the inside with an inflatable or expanding bladder that compacts the laminate against an outer mold line clamshell-type tool. This approach eliminates the tendency of the material to wrinkle as its thickness reduces during consolidation from the layup thickness to the laminate thickness. However, because the Park strut design relies on an interlocking contact of the end fitting with the composite strut body, the strut must use an outer mold line bag against an inner mold line washout tool.

Figure 3.3.1-2 summarizes the strut body fabrication processes. These processes are generally applicable to both demo struts #1 and #2.

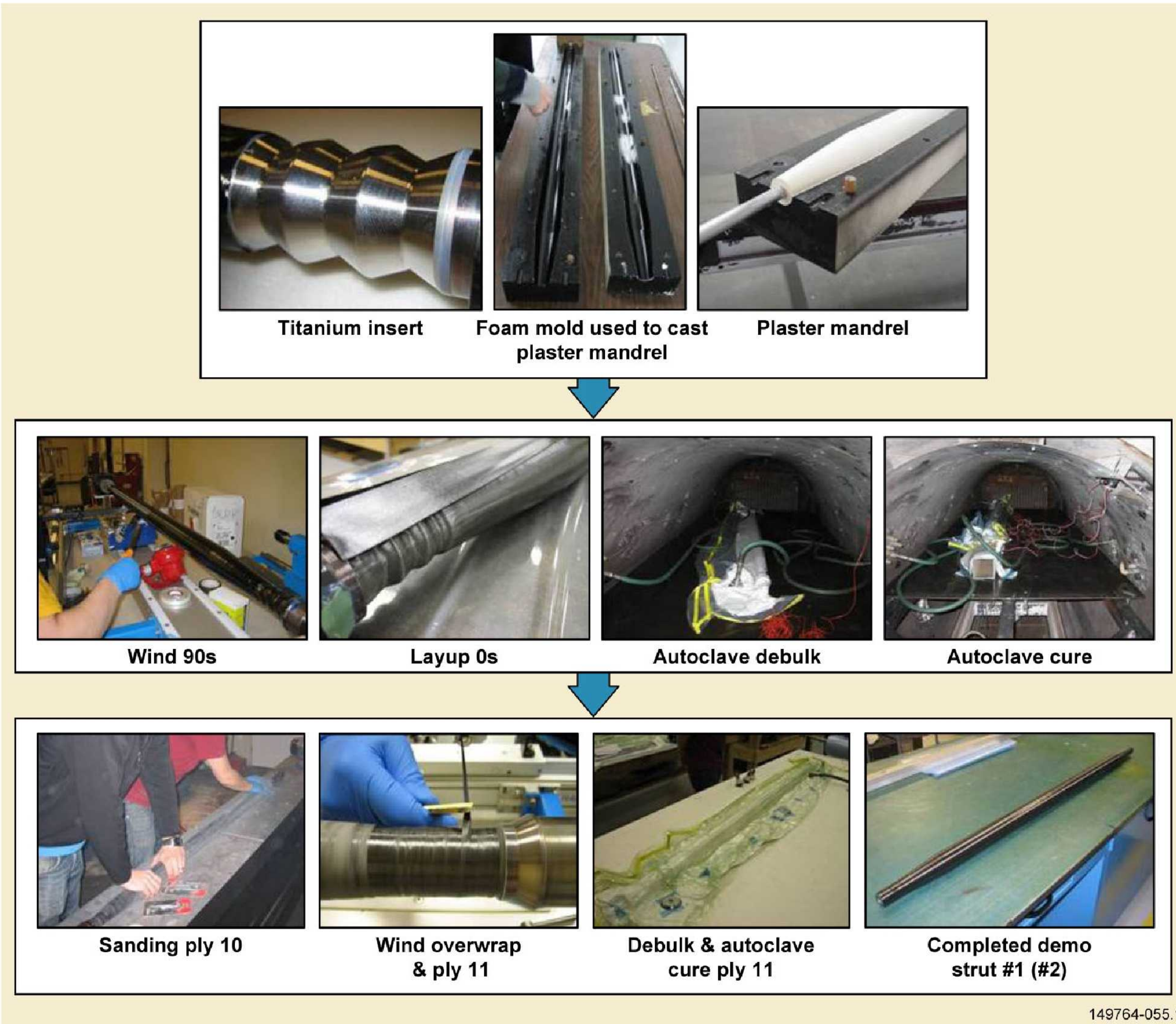

Figure 3.3.1-2. Strut Body Fabrication Processes

All materials used in the fabrication of the demo struts were procured commercially, and prepreg material certifications were per Hexcel internal specifications (HS-AD-971A Rev 4 in the case of the demo struts).

Park inserts are machined from commercially procured annealed 6Al-4V titanium. No passivation, penetrant inspection, or cleaning processes are performed. Insert fabrication was per Park standard process described above. Figure 3.3.1-3 shows one of the resulting inserts.

Figure 3.3.1-3. Titanium Insert

Completed demonstration parts are shown in figure 3.3.1-4.

Figure 3.3.1-4. Demo Struts #1 and #2

4.0 CONCLUSION

The objective of this task order was to perform an analytical study of two structurally efficient, full-scale, tapered composite struts, and to fabricate a subscale strut demonstration article. The approach was to leverage and extend recent experience on a Space Shuttle composite strut development program.

The first step of the analytical study identified design requirements and considerations as applicable to the analytical study, a production program, and the demonstration strut. Using these requirements and considerations, detailed design and stress analysis determined the optimum (minimum) weight of the full-scale struts. One full-scale strut was required to carry a 44,000-lb compression load and have a 135-inch pin-to-pin length. The second strut was required to carry a compression load of 110,000 lb and have a pin-to-pin length of 127 inches.

The design of the demonstration strut was selected from a set of existing designs created during the Shuttle composite strut program. Two approximately half-scale demo struts were fabricated by Park Aerospace Structures, which participated in the Shuttle composite strut program. The first demo strut was fabricated using a higher-cost single-ply autoclave debulk schedule with the objective of achieving the highest possible laminate quality. Thermography inspection was performed on the first demo strut and on a strut fabricated using the Park standard nonautoclave process. The results were used to select the debulk schedule for the second demo strut. Consequently, the second strut was fabricated using a lower-cost debulk schedule that combined autoclave and shrink tape debulking with the objective of balancing fabrication cost and laminate quality. The two demo struts and Park standard strut were nondestructively inspected with an ultrasonic scan. The results identified distinctive indications in the Park standard strut that were less pronounced or absent in the demo struts.

Based on the experience from the fabrication of the demo struts, various process improvements were identified and are recommended to be implemented during the fabrication of a future full-scale strut test article. These improvements will likely improve the traceability and repeatability of the full-scale strut fabrication process, and the resulting quality of the strut laminate. These improvements may in turn improve laminate mechanical properties and further reduce strut weight.

REPORT DOCUMENTATION PAGE	*Form Approved* *OMB No. 0704-0188*

1. REPORT DATE *(DD-MM-YYYY)*	**2. REPORT TYPE**	**3. DATES COVERED** *(From - To)*
01- 05 - 2010	Contractor Report	August 7, 2008 - November 21, 2008

4. TITLE AND SUBTITLE	**5a. CONTRACT NUMBER**
Design of Structurally Efficient Tapered Struts	NNL04AA11B
	5b. GRANT NUMBER
	5c. PROGRAM ELEMENT NUMBER
6. AUTHOR(S)	**5d. PROJECT NUMBER**
Messinger, Ross	**5e. TASK NUMBER** NNL08AD08T
	5f. WORK UNIT NUMBER 727950.04.05.23

7. PERFORMING ORGANIZATION NAME(S) AND ADDRESS(ES)	**8. PERFORMING ORGANIZATION REPORT NUMBER**
NASA Langley Research Center Hampton, VA 23681-2199 The Boeing Company 5302 Bolsa Avenue Huntington Beach, CA 92647-2099	PWDM08-0021

9. SPONSORING/MONITORING AGENCY NAME(S) AND ADDRESS(ES)	**10. SPONSOR/MONITOR'S ACRONYM(S)**
National Aeronautics and Space Administration Washington, DC 20546-0001	NASA
	11. SPONSOR/MONITOR'S REPORT NUMBER(S) NASA/CR-2010-216698

12. DISTRIBUTION/AVAILABILITY STATEMENT
Unclassified - Unlimited
Subject Category 39
Availability: NASA CASI (443) 757-5802

13. SUPPLEMENTARY NOTES

Langley Technical Monitor: Dawn C. Jegley

14. ABSTRACT

This report describes the analytical study of two full-scale tapered composite struts. The analytical study resulted in the design of two structurally efficient carbon/epoxy struts in accordance with NASA-specified geometries and loading conditions. Detailed stress analysis was performed of the insert, end fitting, and strut body to obtain an optimized weight with positive margins. Two demonstration struts were fabricated based on a well-established design from a previous Space Shuttle strut development program.

15. SUBJECT TERMS
Composites; Graphite; Structural efficiency; Buckling

<table>
<tr><th colspan="3">16. SECURITY CLASSIFICATION OF:</th><th rowspan="2">17. LIMITATION OF ABSTRACT</th><th rowspan="2">18. NUMBER OF PAGES</th><th>19a. NAME OF RESPONSIBLE PERSON</th></tr>
<tr><th>a. REPORT</th><th>b. ABSTRACT</th><th>c. THIS PAGE</th><td>STI Help Desk (email: help@sti.nasa.gov)</td></tr>
<tr><td>U</td><td>U</td><td>U</td><td>UU</td><td>53</td><td>19b. TELEPHONE NUMBER (Include area code)
(443) 757-5802</td></tr>
</table>